Soil Biology and Biochemistry 127 (2018) 187–199

Contents lists available at ScienceDirect

Soil Biology and Biochemistry

journal homepage: www.elsevier.com/locate/soilbio

Probing soil nitrification and nitrate consumption using $\Delta^{17}O$ of soil nitrate

Zhongjie Yu*, Emily M. Elliott

Department of Geology and Environmental Science, University of Pittsburgh, Pittsburgh, PA, 15260, USA

ARTICLE INFO

Keywords:
$\Delta^{17}O$
Nitrification
Nitrate consumption
Dual nitrate isotopes
Denitrification
Snowmelt

ABSTRACT

Recent analytical and conceptual advances related to the nitrate (NO_3^-) ^{17}O anomaly ($\Delta^{17}O$) have opened the door to a new method that probes soil nitrification and NO_3^- consumption using $\Delta^{17}O$ of soil NO_3^-. Because biological NO_3^- production and consumption processes in soil obey the mass-dependent fractionation law, $\Delta^{17}O$ of soil NO_3^-, an index of excess ^{17}O over that expected from ^{18}O, can be used to trace gross nitrification and NO_3^- consumption in a way analogous to the $^{15}NO_3^-$ tracer typically employed in studies of soil NO_3^- cycling. Moreover, coupling $\Delta^{17}O$ with the dual NO_3^- isotopes ($\delta^{15}N$ and $\delta^{18}O$) at natural abundances offers additional valuable insights into mechanisms that underlie soil NO_3^- dynamics. In this study, we conducted both laboratory and field experiments to assess the use of $\Delta^{17}O$-NO_3^- for tracing soil nitrification and NO_3^- consumption. Soil samples spanning a wide range of physical and chemical properties were sampled from four sites for batch incubations and amendments with a $\Delta^{17}O$-enriched NO_3^- fertilizer. After amendments, the triple isotopes ($\delta^{15}N$, $\delta^{18}O$, and $\Delta^{17}O$) of soil NO_3^- were measured periodically and used in a developed $\Delta^{17}O$-based numerical model to simultaneously derive gross rates and isotope effects of soil nitrification and NO_3^- consumption. The measured $\Delta^{17}O$-NO_3^- was also used in the classical isotope dilution model to estimate gross NO_3^- turnover rates. *In situ* field soil sampling was conducted in a temperate upland meadow following snowmelt input of $\Delta^{17}O$-enriched atmospheric NO_3^- to assess the robustness of $\Delta^{17}O$-NO_3^- as a natural tracer. The results show that the temporal dynamics of $\Delta^{17}O$-NO_3^- can provide quantitative information on soil nitrification and NO_3^- consumption. In the laboratory incubations, a wide range of gross nitrification and NO_3^- consumption rates were estimated for the four soils using the $\Delta^{17}O$-based models. The estimated rates are well within the range reported in previous ^{15}N tracer-based studies and not sensitive to oxygen isotopic fractionations during nitrification and NO_3^- consumption. Coupling $\Delta^{17}O$-NO_3^- with the dual NO_3^- isotopes using the numerical model placed strong constraints on the $\delta^{15}N$ and $\delta^{18}O$ endmembers of nitrification-produced NO_3^- and revealed soil-specific N isotope effects for nitrification and NO_3^- consumption, consistent with the inferred differences in soil microbial community structure among these soils. Non-zero $\Delta^{17}O$-NO_3^- values, up to 4.7‰, were measured in the meadow soil following the snowmelt event. Although soil heterogeneity in the field prevents quantitative rate estimation using $\Delta^{17}O$-NO_3^-, active NO_3^- cycling via co-occurring nitrification and denitrification was revealed by the covariations in the triple NO_3^- isotopes. Integrating the field observations with the incubation results uncovered isotopic overprinting of nitrification on denitrification in the surface soil following the snowmelt, which has important implications for explaining the discrepancies between field- and laboratory-derived isotope systematics of denitrification. We conclude that $\Delta^{17}O$-NO_3^- is a conservative and powerful tracer of soil nitrification and NO_3^- consumption and future applications are expected to help disentangle soil NO_3^- cycling complexity at various scales.

1. Introduction

Production and consumption of soil nitrate (NO_3^-) affects a myriad of ecosystem processes, including net primary production and carbon (C) sequestration (LeBauer and Treseder, 2008), ecosystem biodiversity (Tilman et al., 1996), soil acidification (Högberg et al., 2006), surface- and groundwater quality (MacDonald et al., 2002), and production of climatically important trace gases via denitrification (Singh et al., 2010). Determination of soil nitrification and NO_3^- consumption rates is therefore critical for gauging nitrogen (N) retention and loss in ecosystems and its response to the intensified N release from anthropogenic activities (Galloway et al., 2008).

Since the landmark work by Kirkham and Bartholomew (1954), the ^{15}N isotopic pool dilution has been the most accessible means for

* Corresponding author..
E-mail address: zhy35@pitt.edu (Z. Yu).

https://doi.org/10.1016/j.soilbio.2018.09.029
Received 29 June 2018; Received in revised form 26 September 2018; Accepted 27 September 2018
Available online 29 September 2018
0038-0717/

determining gross nitrification and NO_3^- consumption rates in soil. The principal of this technique is based on isotopic labeling of the soil NO_3^- pool with $^{15}NO_3^-$. Gross production and consumption rates can then be estimated from concurrent $^{15}NO_3^-$ dilution by NO_3^- production at natural abundance isotopic composition and disappearance of the $^{15}NO_3^-$ tracer by NO_3^- consumption processes, such as microbial NO_3^- assimilation and denitrification (Hart et al., 1994; Stark and Hart, 1997; Booth et al., 2005). Further method development has expanded on the ^{15}N dilution concept by combining ^{15}N labeling of multiple soil N pools (e.g., NO_3^-, ammonium (NH_4^+) and organic N) with process-based model analysis to trace N fluxes between various product pools, allowing a more complete inquiry into soil NO_3^- dynamics and its role in the soil N cycle (Myrold and Tiedje, 1986; Mary et al., 1998; Müller et al., 2004). However, while ^{15}N tracer-based methods operated in the short term are a powerful tool for measuring gross N transformation rates, they may not be able to provide information that accounts for longer-term variations in N cycling in a heterogeneous soil environment (Groffmann et al., 1993). Moreover, with the ^{15}N tracer-based techniques, it remains challenging and laborious to quantify denitrification, which can possibly represent a significant portion of gross NO_3^- consumption rates (Groffman et al., 2006; Morse et al., 2015).

The natural abundance stable isotope ratios of nitrogen ($^{15}N/^{14}N$) and oxygen ($^{18}O/^{16}O$) in NO_3^- (notated as $\delta^{15}N\text{-}NO_3^-$ and $\delta^{18}O\text{-}NO_3^-$, respectively) are increasingly used to differentiate sources and track biogeochemical transformations acting on NO_3^- at various spatio-temporal scales (Granger and Wankel, 2016; Denk et al., 2017). The unique power of the dual NO_3^- isotopes stems from the distinct isotopic fractionations associated with NO_3^- production and consumption processes, which arise due to relative differences in mass of the involved isotopically substituted N and O species (Casciotti et al., 2013). Laboratory studies using bacterial cultures and soil incubations have revealed strong isotopic discrimination against ^{15}N for autotrophic nitrification (Mariotti et al., 1981; Casciotti et al., 2003; Yun and Ro, 2014), suggesting that nitrification draws down $\delta^{15}N\text{-}NO_3^-$ to values significantly lower than $\delta^{15}N$ of NH_4^+ and organic N in NH_4^+-rich soil (Hall et al., 2016). Nitrification also imprints a characteristic $\delta^{18}O$ to NO_3^- that reflects kinetic and equilibrium isotope effects during incorporation of the three O atoms from soil H_2O and O_2 into nitrified NO_3^- (Casciotti et al., 2010; Buchwald and Casciotti, 2010). Consequently, as nitrification-produced NO_3^- usually has $\delta^{18}O$ values much lower than NO_3^- deposited from the atmosphere, $\delta^{18}O\text{-}NO_3^-$ measurement can be used to differentiate these two major NO_3^- sources of natural ecosystems at various scales (Mayer et al., 2001; Oelmann et al., 2007; Fang et al., 2012). On the other hand, assimilatory and dissimilatory NO_3^- reduction impart enrichment of $\delta^{15}N\text{-}NO_3^-$ and $\delta^{18}O\text{-}NO_3^-$ in pure culture studies (Granger et al., 2008, 2010) and soil incubations (Mariotti et al., 1981; Houlton et al., 2006; Fang et al., 2015), which can be used as a diagnostic signal of NO_3^- consumption (Granger and Wankel, 2016). Importantly, the isotope effects for denitrification uncovered in laboratory observations are significantly larger than those for NO_3^- assimilation (Denk et al., 2017). This large kinetic fractionation by denitrification has been exploited in isotope models to assess patterns and controls on denitrification at the watershed scale by assuming that elevated $\delta^{15}N$ of soil and stream water NO_3^- is predominantly driven by denitrification (Houlton et al., 2006; Fang et al., 2015). However, given that the dual isotope-based model estimates are often highly sensitive to uncertainties in the relevant isotope effects (Fang et al., 2015), the dual NO_3^- isotopes are best suited for constraining relative rather than absolute rates of NO_3^- production and consumption (Casciotti et al., 2013).

Recent developments in the field of NO_3^- ^{17}O anomaly has provided a new means by which ambiguities in NO_3^- dynamics inferred from the dual NO_3^- isotope measurements may be clarified (Michalski et al., 2002; Kaiser et al., 2007). Given the three stable isotopes of O (i.e., ^{16}O, ^{17}O, and ^{18}O), fractionation of $^{17}O/^{16}O$ relative to $^{18}O/^{16}O$ in a normal O isotope fractionation process is proportional to the mass difference between the respective O isotopologues, and this is referred as mass-dependent isotopic fractionation (see Section 2.1 for more details) (Thiemens, 2006). Atmospheric NO_3^- is known to contain an anomalous ^{17}O excess over that expected based on ^{18}O abundances (Michalski et al., 2003). This deviation from the mass-dependent fractionation is attributed to O atom transfer from ozone during the formation of atmospheric NO_3^- (Thiemens, 2006) and quantified by a $\Delta^{17}O$ notation (see Section 2.1 for more details) (Miller, 2002; Young et al., 2002). Because the production of nonzero $\Delta^{17}O\text{-}NO_3^-$ values is strictly a photochemical effect, post-depositional NO_3^- consumption processes in soil, such as denitrification and NO_3^- assimilation, obey the mass-dependent fractionation law, leaving the $\Delta^{17}O\text{-}NO_3^-$ nearly unaltered (Michalski et al., 2004). On the other hand, deposition-derived $\Delta^{17}O\text{-}NO_3^-$ signals in soil can be diluted by nitrification-produced NO_3^-, which has $\Delta^{17}O \approx 0$ (Michalski et al., 2004). Therefore, $\Delta^{17}O\text{-}NO_3^-$ has great potential to resolve NO_3^- dynamics in a manner analogous to $^{15}NO_3^-$ tracer studies (Michalski et al., 2004). Nevertheless, while $\Delta^{17}O\text{-}NO_3^-$ has been increasingly used as an indicator of atmospheric NO_3^- deposition at the watershed scale (Riha et al., 2014; Rose et al., 2015; Fang et al., 2015), its quantitative use in measuring gross nitrification and NO_3^- consumption rates has not been explored in soil systems, nor have its mechanistic couplings with $\delta^{15}N\text{-}NO_3^-$ and $\delta^{18}O\text{-}NO_3^-$.

In this proof-of-concept study, we investigated the effectiveness of $\Delta^{17}O\text{-}NO_3^-$ for probing soil nitrification and NO_3^- consumption through developing a $\Delta^{17}O$-based numerical model. Laboratory soil incubations were conducted where soil samples spanning a wide range of properties were amended with a sodium NO_3^- fertilizer mined in the Atacama Desert, Chile (Allganic Nitrogen Plus 15-0-2, SQM North America Corp., USA; similar products, searchable as “Chilean Nitrate” or “Chile Saltpeter” are for sale through many other vendors). Since this NO_3^- fertilizer was derived from atmospheric NO_3^- deposited over thousands of years, it has a high $\Delta^{17}O\text{-}NO_3^-$ (18.6 ± 0.1‰, n = 4). After the NO_3^-amendment, the triple isotopes ($\delta^{15}N$, $\delta^{18}O$, and $\Delta^{17}O$) of soil NO_3^- was measured periodically to characterize gross soil nitrification and NO_3^- consumption using the numerical model. Because $\Delta^{17}O\text{-}NO_3^-$ is expected to behave similarly as the $^{15}NO_3^-$ tracer, the measured $\Delta^{17}O\text{-}NO_3^-$ was also used in the classical isotope dilution model to estimate gross NO_3^- turnover rates. *In situ* field soil sampling was conducted in a temperate upland meadow following snowmelt input of $\Delta^{17}O$-enriched NO_3^- to the surface soil to assess the usefulness of $\Delta^{17}O\text{-}NO_3^-$ as a natural tracer of soil NO_3^- dynamics. We hypothesize that coupled measurement and process-based modeling of $\Delta^{17}O\text{-}NO_3^-$ can be used to simultaneously quantify gross rates and isotope effects of soil nitrification and NO_3^- consumption and thus offers a new lens through which to view the soil NO_3^- biogeochemistry.

2. Materials and methods

2.1. Mass-dependent fractionation and definition of $\Delta^{17}O$

The detailed theoretical basis of mass-dependent fractionation and derivation of the $\Delta^{17}O$ notation have been reviewed by Miller (2002), Young et al. (2002), and Kaiser et al. (2004). A brief summary is provided here to ease the model description and interpretation of the soil $\Delta^{17}O\text{-}NO_3^-$ data.

The mass differences between the three O isotopes impact their partitioning rates between chemical species and phases, resulting in subtle, albeit measurable, changes in the minor/major isotope ratios ($^{17}R = {}^{17}O/{}^{16}O$ and $^{18}R = {}^{18}O/{}^{16}O$), known as isotopic fractionation. The degree of isotopic fractionation in kinetic processes can be quantified by a kinetic fractionation factor (α_k), which is defined by the instantaneous change in the isotope ratio of the reaction product (R_P) at a given substrate isotope ratio (R_S): $\alpha_k = R_S/R_P$. In equilibrium reactions, isotope ratios of two species, A and B, at equilibrium can be

related by an equilibrium fractionation factor, $\alpha_{eq} = R_A/R_B$. By convention, isotopic fractionation can also be expressed in units of ‰ as an isotope effect (ε): $\varepsilon = (\alpha\text{-}1) \times 1000$. For both kinetic and equilibrium fractionations of the three O isotopes, the isotopic fractionation factors for ^{17}R ($^{17}\alpha$) and ^{18}R ($^{18}\alpha$) are related by the mass-dependent fractionation law:

$$^{17}\alpha = (^{18}\alpha)^{\beta} \quad (1)$$

where β is the three-isotope exponent determined exclusively by the masses of the respective O isotopologues involved in the reaction. Importantly, β is not equal to a single value but varies generally between 0.51 and 0.53 for different O fractionation processes (Miller, 2002; Young et al., 2002). A value of 0.52, however, is chosen as a starting point for all the relevant processes considered in this study (e.g., O incorporation during nitrification, O exchange between H_2O and nitrite (NO_2^-), and NO_3^- consumption; see Section 2.3 for more details), consistent with previous studies on $\Delta^{17}O\text{-}NO_3^-$ in terrestrial and aquatic ecosystems (Michalski et al., 2004; Riha et al., 2014; Rose et al., 2015).

With a β of 0.52, mass-dependent fractionations of the three O isotopes can be represented by a single curve on the O three-isotope plot in which isotope ratios (^{17}R and ^{18}R) are expressed as fractional differences from a reference material ($^{17}R_{ref}$ and $^{18}R_{ref}$) lying on the same curve (i.e., Vienna Standard Mean Ocean Water (VSMOW) in this study) (Miller, 2002):

$$\frac{^{17}R}{^{17}R_{ref}} = \left(\frac{^{18}R}{^{17}R_{ref}}\right)^{0.52} \quad (2)$$

By using delta notation ($\delta = [(R/R_{ref})\text{-}1] \times 1000$, in unit of ‰) and natural log transformation, Equation (2) becomes:

$$\ln\left(\frac{\delta^{17}O}{1000} + 1\right) = 0.52 \ln\left(\frac{\delta^{18}O}{1000} + 1\right) \quad (3)$$

Thus, a plot of $\ln(\delta^{17}O/1000 + 1)$ against $\ln(\delta^{18}O/1000 + 1)$ produce a straight line of slope 0.52 in the O three-isotope space, representing the mass-dependent fractionation law. On this basis, anomalous ^{17}O excess or deficiency ($\Delta^{17}O$), characterized by the departure from the mass-dependent fractionation line as a result of mass-independent isotope effects (e.g., photochemical ozone formation), is defined in delta notation as:

$$\Delta^{17}O = \left[\ln\left(\frac{\delta^{17}O}{1000} + 1\right) - 0.52 \ln\left(\frac{\delta^{18}O}{1000} + 1\right)\right] \times 1000 \quad (4)$$

Following Equation (4), two considerations must be kept in mind when interpreting $\Delta^{17}O\text{-}NO_3^-$ data. First, because $\Delta^{17}O$ defined in Equation (4) is not linear in $\delta^{18}O$ or $\delta^{17}O$, simple mass balance and mixing calculations with $\Delta^{17}O$ should be regarded as approximations (Kaiser et al., 2004). Second, given that β (i.e., the slope of the mass-dependent fractionation line) may not be equal to a single value for a complex fractionation process involving multiple steps or O species (e.g., nitrification), $\Delta^{17}O$ values very close to zero should not be construed as indication of mass-independent processes (Young et al., 2002).

2.2. $\Delta^{17}O$-based numerical model of soil nitrification and nitrate consumption

Given that the tracing power of $\Delta^{17}O\text{-}NO_3^-$ relies on mass-dependent fractionation law and that nitrification is a multi-step, multi-phase fractionation process, it is important to carefully and explicitly evaluate the effects of isotopic fractionations on $\Delta^{17}O\text{-}NO_3^-$ as a conservative tracer of soil nitrification and NO_3^- consumption. Equally important is to couple $\Delta^{17}O\text{-}NO_3^-$ with the dual NO_3^- isotopes to assess what new insights the triple NO_3^- isotopes can contribute to the NO_3^- biogeochemistry in soil. To meet these needs, a numerical model was devised based on current understanding of the biochemistry and isotopic systematics of nitrification and NO_3^- consumption (Fig. 1).

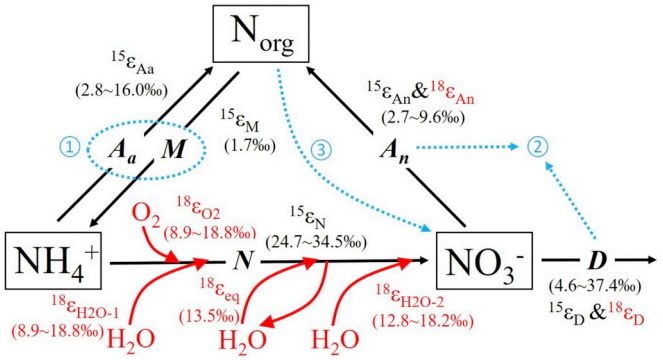

Fig. 1. Conceptual schematic for relevant N transformation processes between the NO_3^-, NH_4^+ and organic N pools. The black arrow lines denote N mass flows. M = gross mineralization; N = gross nitrification with NH_4^+ as the substrate; A_a and A_n = gross microbial assimilation of NH_4^+ and NO_3^-, respectively; D = gross denitrification. Each of these N transformation processes is associated with a kinetic isotope effect ($^{15}\varepsilon$). Characteristic estimates for $^{15}\varepsilon$ are adopted from Denk et al. (2017) and given in parentheses. The red arrow lines denote O incorporation during nitrification through kinetic O extraction from O_2 and H_2O and equilibrium O exchange with H_2O. The estimates for O isotope effects ($^{18}\varepsilon$) associated with the O incorporation are adopted from Granger and Wankel (2016) and given in parentheses. It is assumed that N and O isotope effects for microbial NO_3^- assimilation and denitrification are coupled (i.e., $^{15}\varepsilon = {}^{18}\varepsilon$). The blue dashed arrow lines and cycle illustrate the accommodation of the conceptual model for parameterizing the $\Delta^{17}O$-based numerical model: ① mineralization and NH_4^+ assimilation are combined to be a net flux between the NH_4^+ and organic N pools (i.e., net mineralization); ② microbial NO_3^- assimilation and denitrification are combined to be gross NO_3^- consumption; ③ in cases where the NH_4^+ pool is depleted, NO_3^- production is directly modeled from the organic N pool (i.e., coupled mineralization and nitrification). (For interpretation of the references to color in this figure legend, the reader is referred to the Web version of this article.)

Three soil N pools are considered in the numerical model: organic N, NH_4^+, and NO_3^- (Mary et al., 1998; Müller et al., 2004) (Fig. 1). Mineralization of organic N produces NH_4^+, which can be returned to the organic N pool as microbial biomass N via microbial NH_4^+ assimilation or nitrified to NO_3^-, while NO_3^- can be consumed via microbial assimilation and denitrification. Each of these N transformation processes is associated with a kinetic N isotope effect (see Denk et al. (2017) for a review) (Fig. 1). During the two-step process of nitrification, the oxidation of NH_4^+ to NO_2^- incorporates one O atom from O_2 and one from H_2O; the subsequent oxidation of NO_2^- to NO_3^- incorporates an O atom derived from H_2O (Fig. 1). Recent work has revealed kinetic isotope effects associated with enzymatic incorporation of each of the three O atoms into the nitrified NO_3^-, as well as the isotopic equilibrium of O atoms between NO_2^- and H_2O during the first oxidation step (see Granger and Wankel (2016) for a review) (Fig. 1). Moreover, NO_3^- consumption processes fractionate the O isotopes of NO_3^- to a similar degree as the N isotopes (Fig. 1).

The numerical model was parameterized with following considerations (Fig. 1). First, NO_2^- is not explicitly included in the model because it was not in significant concentrations in either the incubation experiments or the field sampling. Therefore, N and O isotope effects for NO_2^- oxidation to NO_3^- are considered not expressed. Second, mineralization and NH_4^+ assimilation fluxes are combined to be a net mineralization flux between the organic N and NH_4^+ pools to lower the number of unknowns in the model such that the model system is determined (i.e., number of unknowns not exceed number of measured variables (Mary et al., 1998)). Third, in cases where the soil NH_4^+ pool is depleted due to tightly coupled net mineralization and nitrification, NO_3^- production and its N isotope effect are modeled from the organic N pool. Fourth, NO_3^- assimilation and denitrification are not

partitioned in the model. Instead, a N isotope effect is estimated for overall gross NO_3^- consumption. Given the previous experimental evidence that N isotopic fractionation is significantly stronger during denitrification than during NO_3^- assimilation, the estimated bulk N isotope effect reflects the relative importance of denitrification (Houlton et al., 2006; Fang et al., 2015). Finally, and most importantly, the fractionations of $^{17}O/^{16}O$ and $^{18}O/^{16}O$ for all the kinetic and equilibrium O fractionation processes in the model are related using the mass dependent fractionation law (i.e., Equation (1)).

Using the model structure described above, a set of differential equations was constructed to simulate the N and O isotopologue pools of soil NO_3^- (i.e., ^{14}N, ^{15}N, ^{16}O, ^{17}O, and ^{18}O) and NH_4^+ (i.e., ^{14}N and ^{15}N). While the kinetics of the net mineralization is fixed to be zero-order, nitrification and NO_3^- consumption can either follow zero- or first-order kinetics. Under default settings the model simulates nitrification using the fractionations of $^{18}O/^{16}O$ summarized by Granger and Wankel (2016) (i.e., midrange values shown in Fig. 1), 23.5‰ and −10‰ for $\delta^{18}O$ of soil O_2 and H_2O, respectively, and 0.2 for the fractional O exchange between NO_2^- and H_2O catalyzed by nitrifiers (Casciotti et al., 2010). The mathematical formulation of the model adopting zero-order kinetics for all the N transformation processes is provided in Appendix A.

We applied the model to test the robustness of $\Delta^{17}O\text{-}NO_3^-$ in tracing nitrification and NO_3^- consumption in two specific cases. First, zero-order rates of gross nitrification and NO_3^- consumption were fitted using the measured time series of soil NO_3^- concentration and $\Delta^{17}O\text{-}NO_3^-$. To examine the conservative nature of $\Delta^{17}O\text{-}NO_3^-$ during soil nitrification and NO_3^- consumption, the effects of β, the $\delta^{18}O$ of the O sources, and the assumed O isotope effects on the rate estimates were investigated by simultaneously varying these factors over their respective ranges of possible values (Table S1) using a Monte Carlo routine (1000 times). In the second case, process rates (or rate constants) and N isotope effects of the net mineralization, nitrification, and NO_3^- consumption were optimized using the measured concentrations and $\delta^{15}N$ values of soil NH_4^+ and NO_3^- in tandem with $\Delta^{17}O\text{-}NO_3^-$. To uniquely solve this model system, concentration and $\delta^{15}N$ of soil organic N are required. However, because soil organic N was not measured in this study, we assumed it can be approximated by the total soil N in terms of pool size and $\delta^{15}N$ value similar to previous natural abundance studies of soil N isotopes (e.g., Decock and Six, 2013; Snider et al., 2015; Hall et al., 2016). In both cases, the isotopologue-specific differential system of equations was solved numerically using a Runge-Kutta method with a variable time step (Solver ode45, Matlab, Mathworks, USA) and the measured initial values of the isotopologue pools. The resultant isotopologue abundances were converted to concentrations and isotopic compositions (in delta notation) for interpretation. A non-linear optimization applying Trust-Region-Reflective least squares algorithm (Matlab, Mathworks, USA) was then used to find the unknown N process rates (or rate constants) and N isotope effects that minimize the quadratic weighted error between predicted and measured results (Mary et al., 1998). To avoid local minima, the optimization procedure was repeated three times with different initial values for fitted parameters and only considered successful when the same set of parameters was obtained in the three replicate runs. Approximate 95% confidence intervals were calculated for parameter estimates using an error covariance matrix.

2.3. $\Delta^{17}O$ dilution model of soil nitrification and nitrate consumption

The classical isotope dilution equations (Kirkham and Bartholomew, 1954; Smith et al., 1994) were also applied to calculate gross soil nitrification and NO_3^- consumption rates:

$$R_N = -\frac{[NO_3^-]_2 - [NO_3^-]_1}{t_2 - t_1} \times \frac{\ln\left(\frac{E_2}{E_1}\right)}{\ln\left(\frac{[NO_3^-]_2}{[NO_3^-]_1}\right)} \quad (5)$$

$$R_{NC} = -\frac{[NO_3^-]_2 - [NO_3^-]_1}{t_2 - t_1} \times \left(1 + \frac{\ln\left(\frac{E_2}{E_1}\right)}{\ln\left(\frac{[NO_3^-]_2}{[NO_3^-]_1}\right)}\right) \quad (6)$$

where R_N and R_{NC} are gross nitrification and NO_3^- consumption rates (μg $N{\cdot}g^{-1}{\cdot}d^{-1}$), respectively; $[NO_3^-]$ is the soil NO_3^- concentration (μg $N{\cdot}g^{-1}$); the subscripts 1 and 2 denote two soil sampling times t_1 and t_2, respectively. In the case of $^{15}NO_3^-$ tracer studies, E denotes excess ^{15}N over natural abundance. Analogously, in our case, E is $\Delta^{17}O\text{-}NO_3^-$, an index of excess ^{17}O over that expected from ^{18}O and the mass-dependent fractionation law. A derivation of Equations (5) and (6) with $\Delta^{17}O\text{-}NO_3^-$ as the input is given in Appendix B. Importantly, applying $\Delta^{17}O\text{-}NO_3^-$ with the isotope dilution model implicitly assumes that: (1) both nitrification and NO_3^- consumption can be described by zero-order kinetics during measurement intervals, (2) $\Delta^{17}O\text{-}NO_3^-$ is linear in terms of mixing, (3) nitrification-produced NO_3^- has $\Delta^{17}O = 0$, and (4) NO_3^- consumption does not in itself alter $\Delta^{17}O\text{-}NO_3^-$. While the first assumption is probably met in short-term laboratory incubation experiments (Smith et al., 1994; Davidson et al., 1991), the last three assumptions were tested by comparing the calculated gross nitrification and NO_3^- consumption rates to those estimated using the numerical model.

2.4. Laboratory soil incubations

We sampled soils from four sites in and around Pittsburgh, Pennsylvania, USA: a conventional corn field receiving mineral fertilizers (hereafter, agricultural site), a mowed, poorly drained, grassy, upland meadow in a forest clearing (meadow site), an urban mixed hardwood forest experiencing partial cutting (forest site), and a restored urban riparian floodplain with herbaceous vegetation (riparian site). Importantly, the purpose of sampling soils from four different ecosystems is to achieve a broad range of soil properties and, presumably, soil microbial community structures to test the $\Delta^{17}O$-based models; this is not to be misconstrued as an attempt to assess differences among the ecosystems at a broader level. At each site, soil samples (n = 24) were collected using a stainless-steel corer (5 cm inner diameter) to a depth of 7 cm to form a composite soil sample. Prior to sampling at the forest site, the upper layer (Oi horizon, approximately 5 mm thick) of the forest floor was removed from the sampling area. In the laboratory, fresh soils were sieved by passing through 2 mm sieves and left to air-dry at room temperature (22 °C) for later analyses. Basic characteristics of each soil can be found in Table 1. For the four soils, pH ranged from 5.0 to 5.7. The forest soil was highly humified and had the highest total and organic C content, followed by the riparian, meadow, and agricultural soils. Total N was highest in the forest soil (0.9%) and lowest in the agricultural soil (0.2%), whereas $\delta^{15}N$ of total N was highest in the agricultural soil (5.3‰) and lowest in the meadow soil (2.2‰). Inhibitor-based nitrification (Belser and Mays, 1980) and denitrification (Groffman et al., 1999) potentials were measured within two days before the incubation experiments. Nitrification potential was significantly higher in the forest, riparian, and agricultural soils with high antecedent NO_3^- concentrations than in the meadow soil, where NH_4^+ dominated the inorganic N pool (Table 1). Denitrification potential was 3.6, 8.5, and 9.7 μg $N{\cdot}g^{-1}{\cdot}d^{-1}$ for the meadow, forest, and riparian soils, respectively (Table 1).

To initiate the incubation experiments for the meadow, forest, and riparian soils, 35 g (dry weight equivalent) of the sieved soils were weighted into six sets of 250 mL Nalgene bottles with eight bottles per set. The soils were then fertilized with the Chilean NO_3^- ($\delta^{15}N\text{-}NO_3^-$ = 0.3 ± 0.1‰, $\delta^{18}O\text{-}NO_3^-$ = 55.8 ± 0.1‰) and ammonium

Table 1
Soil characteristics, N transformation rates, and isotope effects estimated using the numerical model in the laboratory incubation experiments.

Soil	Agricultural	Meadow	Forest	Riparian
Soil characteristics[a]				
Taxonomic classification	Alfisol	Ultisol	Ultisol	Entisol
Texture (% sand, % silt, % clay)	silt loam (21, 58, 21)	silty clay loam (31, 67, 2)	silt loam (19, 62, 19)	silt loam (20, 62, 18)
Bulk density ($g{\cdot}cm^{-3}$)	1.22	1.13	0.87	0.92
pH (1:1 water)	5.7	5.0	5.4	5.6
Indigenous soil water content (g $H_2O{\cdot}g^{-1}$)	0.15	0.50	0.42	0.40
Soil water content adopted for incubation (g $H_2O{\cdot}g^{-1}$)[b]	0.22	0.72	0.65	0.57
Total carbon (%)	1.8	6.6	13.2	8.4
Organic carbon (%)	1.8	6.4	9.9	7.5
Total nitrogen (%)	0.2	0.5	0.9	0.5
$\delta^{15}N$ of total nitrogen (‰)	5.3	2.2	3.7	3.9
C:N ratio (mol:mol)	11.4	14.6	17.3	19.6
Antecedent NH_4^+ ($\mu g\ N{\cdot}g^{-1}$)	0.7	19.1	0.7	0.5
Antecedent NO_3^- ($\mu g\ N{\cdot}g^{-1}$)	29.8	2.1	18.7	15.7
Nitrification potential ($\mu g\ N{\cdot}g^{-1}{\cdot}d^{-1}$)	14.6	2.6	21.5	14.7
Denitrification potential ($\mu g\ N{\cdot}g^{-1}{\cdot}d^{-1}$)	NA[c]	3.6	8.5	9.7
Estimated N transformation rates and N isotope effects[d]				
Net mineralization ($\mu g\ N{\cdot}g^{-1}{\cdot}d^{-1}$)[e]	0.90 ± 0.37	2.13 ± 0.11	NA[f]	NA[f]
Gross nitrification ($\mu g\ N{\cdot}g^{-1}{\cdot}d^{-1}$)	9.75 ± 0.15	1.71 ± 0.02	10.32 ± 0.67[f]	5.85 ± 0.22[f]
Gross NO_3^- consumption ($\mu g\ N{\cdot}g^{-1}{\cdot}d^{-1}$)	0.81 ± 0.15	0.75 ± 0.02	5.45 ± 0.67	2.87 ± 0.22
N isotope effect for net mineralization (‰)	0.0 ± 5.0	4.4 ± 3.2	NA[f]	NA[f]
N isotope effect for nitrification (‰)	32.8 ± 1.4	28.4 ± 2.1	1.7 ± 3.1[f]	1.8 ± 2.2[f]
N isotope effect for NO_3^- consumption (‰)	0.0 ± 15.0	8.1 ± 4.9	0.0 ± 5.1	0.2 ± 4.6

[a] Each datum is an average based on three replicate measurements.
[b] Soil water content corresponding to 100% field capacity for the meadow, forest, and riparian soils and 80% for the agricultural soil.
[c] Not available.
[d] The estimated N transformation rates and isotope effects are presented as mean plus and minus margin of error of the 95% confidence interval.
[e] Net mineralization is defined as the net flux of mineralization and NH_4^+ assimilation between the NH_4^+ and organic N pools.
[f] Due to the depletion of the soil NH_4^+pool, gross rates and isotope effects were estimated for the coupled net mineralization and nitrification.

sulfate ($(NH_4)_2SO_4$; $\delta^{15}N\text{-}NH_4^+ = 1.9 \pm 0.3‰$) dissolved in deionized Milli-Q water at the same N concentration to achieve field capacity water content (Table 1) and an initial $\Delta^{17}O\text{-}NO_3^-$ of 5‰. This initial $\Delta^{17}O\text{-}NO_3^-$ signal (5‰) is a direct result of mixing between the Chilean NO_3^- and indigenous NO_3^- in the soils ($\Delta^{17}O\text{-}NO_3^- \approx 0‰$) and consistent with the highest $\Delta^{17}O\text{-}NO_3^-$ (4.7‰) observed at the meadow site during the field snowmelt sampling (see below). The field capacity water content was chosen for the soil incubation to simulate $\Delta^{17}O\text{-}NO_3^-$ input via wet deposition, which often leads to concurrent (semi-)saturated soil conditions. Moreover, NH_4^+ addition was also used here, as NH_4^+ is often found to present in comparable concentrations as NO_3^- in wet deposition (Li et al., 2016). The N addition to these soils increased the soil NO_3^- concentrations by about 37%, while the soil NH_4^+ concentrations were increased by < 5% to > 100%, depending on the antecedent concentrations (Table 1). Long-term $\delta^{18}O$ of the Milli-Q water produced in our lab is −10.1 ± 0.2‰ (n = 12). After the amendment, the bottles were sealed with Parafilm with seven pin holes for gas exchange and incubated in the dark at room temperature. Soil extractions were carried out about 0.5, 12, 24, 48, 72, and 96 h after the fertilizer application. At each extraction, the eight replicate samples were divided into two groups and four of them were extracted for NH_4^+ determination using 175 mL of 2 M KCl. We followed Costa et al. (2011) to extract soil NO_3^- for determination of concentration and the triple NO_3^- isotopes. Each of the four remaining bottles was combined with 70 mL deionized Milli-Q water and vortexed for 10 min at 3200 rpm. The slurry was then centrifuged for 10 min at 2000 rpm, and the resultant supernatant was filtered through a sterile 0.2 μm filter. The agricultural soil was incubated using a similar protocol in which higher amount of soil (100 g dry weight equivalent), lower soil water content (80% of field capacity; Table 1), less frequent sampling (four times over four days), larger additions of NO_3^- (15 $\mu g\ N{\cdot}g^{-1}$) and NH_4^+ (90 $\mu g\ N{\cdot}g^{-1}$), and higher initial $\Delta^{17}O\text{-}NO_3^-$ (6‰) were adopted for the incubation to accommodate measurements of N trace gas emission in a separate study.

2.5. Field snowmelt sampling

In situ soil sampling was conducted at the meadow site following a snowmelt event. This site was located at a toe-slope position and subject to continuous monitoring of surface soil temperature and water content (5 cm depth) since 2016 (Fig. S1a). Snow precipitation occurred on February 9, 2017, resulting in a maximum snow depth of about 25 cm, equivalent to about 3 cm of snow water, as recorded by the nearest (3 miles) snow monitoring station (PA-SM-3, National Operational Hydrologic Remote Sensing Center, NOAA). Three snowpack samples were collected on February 10 before the onset of the snowmelt. After the completion of the snowmelt, eight soil cores (5 cm inner diameter, 7 cm depth) were collected daily from February 11 through February 15 within a 5 by 5 m square. During this time period, soil experienced temperature fluctuated between 2.5 °C and 6.0 °C and remained nearly saturated (Fig. S1b). The sampled intact soil cores were stored at 4 °C and immediately transported back to the laboratory where they were gently broken up by hands, slightly air-dried, sieved through a 4 mm mesh, and extracted for determination of NO_3^- concentration and the triple NO_3^- isotopes on the same day as previously described.

2.6. Chemical and isotopic analyses

Analyses for NO_3^- and NO_2^- in the soil extracts were carried out on a Dionex Ion Chromatograph ICS-2000 with a precision (1σ based on replicate standard measurements) of ± 5.0 $\mu g\ N{\cdot}L^{-1}$ and ± 2.5 $\mu g\ N{\cdot}L^{-1}$, respectively. NH_4^+-N analyses were carried out on a fluorometer (Trilogy, Turner Designs, USA) using a modified fluorometric OPA method for soil KCl extracts (Kang et al., 2003; Taylor et al., 2007) with a precision of ± 7.0 $\mu g\ N{\cdot}L^{-1}$.

The $\delta^{15}N$ and $\delta^{18}O$ of the extracted soil NO_3^- were measured using the denitrifier method (Sigman et al., 2001; Casciotti et al., 2002). In brief, denitrifying bacteria lacking the nitrous oxide (N_2O) reductase enzyme (*Pseudomonas aureofaciens*) are used to convert 20 nmol of NO_3^- into gaseous N_2O. Using He as a carrier gas, the N_2O is then

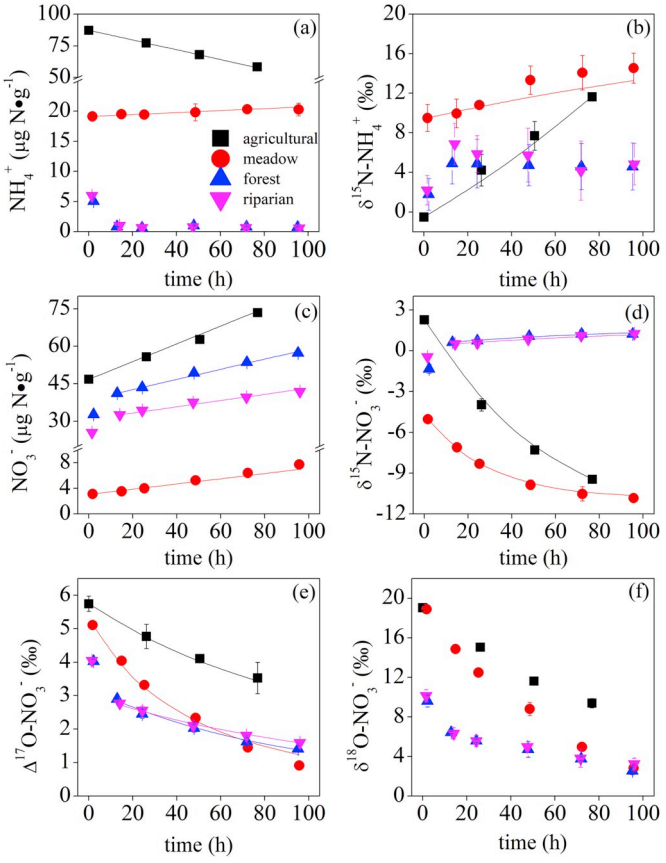

Fig. 2. Measured (symbols) and modeled (lines) concentrations and isotopic compositions of NH_4^+ and NO_3^- after application of the Chilean NO_3^- fertilizer to the four soils in the laboratory incubation experiments. The error bar denotes standard deviation of the replicate measurements. If no bars are evident, the errors were less than the size of the symbol.

purified in a series of chemical traps, cryofocused, and finally analyzed on a GV Instruments Isoprime continuous flow isotope ratio mass spectrometer (CF-IRMS). International NO_3^- reference standards IAEA-N3 and USGS34 were used to calibrate the δ^{15}N measurements, while the δ^{18}O measurements were corrected using IAEA-N3, USGS34, and USGS35. The long-term (n > 100) precision for the δ^{15}N and δ^{18}O analyses are ± 0.3‰ and ± 0.5‰, respectively. The Δ^{17}O of soil NO_3^- was measured using the coupled bacterial reduction and thermal decomposition method described by Kaiser et al. (2007). After converting 200 nmol of soil NO_3^- sample to N_2O, the N_2O was thermally converted to O_2 and N_2 by reduction over a gold surface at 800 °C. The O_2 and N_2 were separated using a 5 Å molecular sieve gas chromatograph and the O_2 was analyzed for δ^{17}O and δ^{18}O by the CF-IRMS. The Δ^{17}O was calculated using Equation (4) and calibrated by USGS34, USGS35, and a 1:1 mixture of USGS34 and USGS35. The precision for Δ^{17}O analysis of USGS35 and the USGS35:USGS34 mixture is ± 0.3‰. According to Kaiser et al. (2007), the measured Δ^{17}O was used in reduction of molecular isotope ratios of N_2O to correct the isobaric interference (i.e., $^{14}N^{14}N^{17}O$ on *m/z* 45) on the δ^{15}N analysis via the denitrifier method. It is noteworthy that while the configuration of our CF-IRMS system does not allow us to precisely measure δ^{15}N of N_2, simultaneous determination of δ^{15}N, δ^{18}O, and Δ^{17}O of NO_3^- using both N_2 and O_2 produced from the N_2O thermal decomposition, as can be achieved by some specialized mass spectrometer systems (e.g., Morin et al. (2009)), in a single run can improve analytical efficiency and circumvent the nonzero Δ^{17}O-induced isobaric interference on the δ^{15}N analysis.

The δ^{15}N of the extracted soil NH_4^+ was measured by coupling the ammonia (NH_3) diffusion method (Zhang et al., 2015) and the hypobromite (BrO^-) oxidation method (Zhang et al., 2007) with the denitrifier method (Felix et al., 2013). Briefly, an aliquot of soil KCl extract having 20–60 nmol NH_4^+ was pipetted into a 20 mL serum vial containing an acidified glass fiber disk. The solution was made alkaline by adding Magnesium oxide (MgO) to volatilize NH_3 which is subsequently captured on the acidic disk. After removal of the disk, NH_4^+ was eluted using deionized Milli-Q water, diluted to 10 μM, oxidized by BrO^- to NO_2^-, and finally measured for δ^{15}N as NO_2^- at 20 nmol using the denitrifier method as described above. International NH_4^+ reference standards IAEA-N1, USGS25, and USGS26 undergone the same preparation procedure as the soil samples were used along with the NO_3^- reference standards to correct for blanks and instrument drift. The precision for the δ^{15}N-NH_4^+ analysis is ± 0.5‰.

2.7. Statistical analyses

We evaluated the significant difference between the model estimates (i.e., gross rates and isotope effects of nitrification and NO_3^- consumption) by examining the overlap between the associated 95% confidential intervals and consider the result conservative (Schenker and Gentleman, 2001). Pearson's correlation coefficient was used to detect significant relationships among independent variables. Simple linear regression was used to examine relationships among NO_3^- concentration and triple NO_3^- isotopes during the laboratory incubations and field snowmelt samplings. One-sample *t*-test was used to determine whether Δ^{17}O-NO_3^- values measured on each field sampling day was significantly different from zero. The significant differences in Δ^{17}O-NO_3^- values between different field sampling days was detected using a one-way ANOVA with a pairwise Bonferroni test. All the statistical analyses were conducted using MATLAB (Mathworks, USA) and evaluated at the 0.05 level of significance.

3. Results

3.1. Laboratory soil incubations

Throughout this paper, soil N concentrations and transformation rates are expressed on the basis of soil oven-dry weight. For all the four soils studied in the laboratory, the NO_3^- concentrations increased significantly over the incubation period (Fig. 2c). Nitrite was detectable in the agricultural, forest, and riparian soils but its concentrations did not exceed 1% of the NO_3^- concentrations throughout the incubations. The large increase in the NO_3^- concentration during the incubation period in the agricultural soil was accompanied by significant declines in the NH_4^+ concentration (Fig. 2a) and the δ^{15}N-NO_3^- (Fig. 2d), whereas the δ^{15}N-NH_4^+ increased during the incubation (Fig. 2b). Declining δ^{15}N-NO_3^- and increasing δ^{15}N-NH_4^+ were also observed for the meadow soil (Fig. 2b and d), although the NH_4^+ concentration remained relatively stable throughout the experimental period (Fig. 2a). The added NH_4^+ was rapidly consumed within 12 h after the amendment in the forest and riparian soils (Fig. 2a), leading to a steep increase in the NO_3^- concentrations and δ^{15}N-NO_3^- values (Fig. 2c and d). Thereafter, the NH_4^+ concentrations were < 1 μg N·g^{-1} and the δ^{15}N values of NO_3^- and NH_4^+ remained relatively constant, despite the steady increases in the NO_3^- concentrations (Fig. 2).

The applied Δ^{17}O-NO_3^- tracer was nearly fully recovered 0.5 h after the amendment in the agricultural and meadow soils, whereas the recovery was only about 80% for the forest and riparian soils (Fig. 2e). For the four soils, Δ^{17}O-NO_3^- values declined progressively by 2.5‰–4.2‰ during the incubation period (Fig. 2e), and the pooled standard deviation of the replicate Δ^{17}O-NO_3^- measurements was ± 0.13‰. A concurrent decrease in δ^{18}O-NO_3^- values was observed for all four soils (Fig. 2f), resulting in positive linear relationships between Δ^{17}O-NO_3^- and δ^{18}O-NO_3^- (Fig. 3b). Δ^{17}O-NO_3^- values also varied linearly with δ^{15}N-NO_3^- values, yet the linear relationships are different

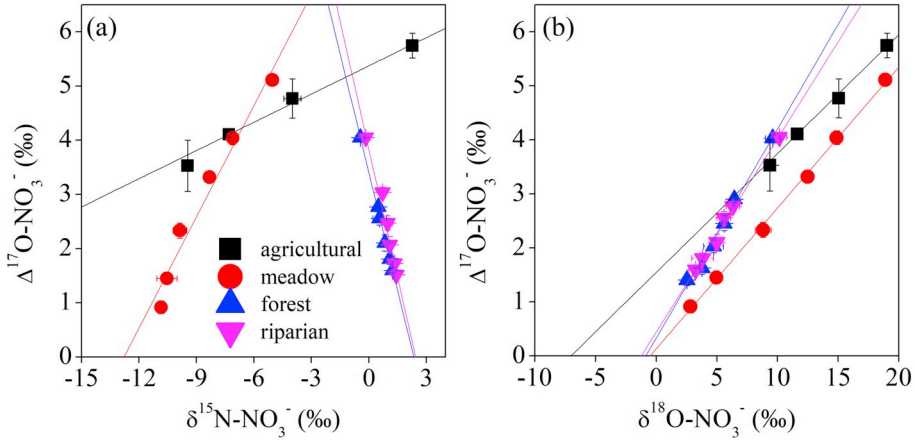

Fig. 3. Relationships between Δ^{17}O-NO_3^- and δ^{15}N-NO_3^- (a) and between Δ^{17}O-NO_3^- and δ^{18}O-NO_3^- (b) in the laboratory incubation experiments. The error bar denotes standard deviation of the replicate measurements. The lines represent linear regression fits for the respective relationships for the four soils.

among the soils: positive for the agricultural and meadow soils and negative for the forest and riparian soils (Fig. 3a).

When applied to every two consecutive soil extractions, a wide range of gross nitrification (1.2–26 μg N·g^{-1}·d^{-1}) and NO_3^- consumption (0.3–8 μg N·g^{-1}·d^{-1}) rates were estimated using the numerical model for the four soils (Fig. 4; Table S2). Sensitivity analysis indicated that the numerically solved rate estimates are stable over the relevant range of β, the δ^{18}O values of O sources (i.e., O_2 and H_2O), and the kinetic and equilibrium O isotope effects during nitrification and NO_3^- consumption (Table S1), with typical standard deviation derived from 1000 Monte Carlo iterations being less than 6% of the simulated mean values for gross nitrification and NO_3^- consumption rates (Figs. S2–S5). Relative to the numerical model, the Δ^{17}O dilution model tended to overestimate gross nitrification and NO_3^- consumption rates by 7.0 ± 3.6% and 17.1 ± 10.8%, respectively, for the four soils (Fig. 4; Table S2).

When the gross rates were optimized by fitting the numerical model to all observations made over the incubations, both nitrification and NO_3^- consumption were better described by zero-order kinetics than by first-order kinetics for the agricultural and meadow soils. Because the NH_4^+ pool was quickly depleted after the amendment in the forest and riparian soils (Fig. 2a), preventing accurate estimation of nitrification through the NH_4^+ pool, zero-order rates of the coupled net mineralization and nitrification were estimated for these two soils using data measured 12 h after the amendment. For all four soils, the observed concentrations and isotopic compositions were well-approximated by the numerical model (Fig. 2). The good quality of fit was confirmed by the high fraction of the total variation explained by the model, as indicated by a $R^2 > 0.95$ for all four soils. The only noticeable difference relative to the standard deviation of the replicate measurements was a slight underestimation of the δ^{15}N-NH_4^+ in the meadow soil during the last three sampling intervals. The estimated gross nitrification rate was higher in the forest (10.32 ± 0.67 μg N·g^{-1}·d^{-1}) and agricultural (9.75 ± 0.15 μg N·g^{-1}·d^{-1}) soils than in the riparian (5.85 ± 0.22 μg N·g^{-1}·d^{-1}) and meadow (1.71 ± 0.02 μg N·g^{-1}·d^{-1}) soils (Table 1). The estimated gross nitrification rates were positively associated with the nitrification potentials among the four soils ($\rho = 0.91$, $P = 0.09$, $n = 4$). Nitrification was associated with a large N isotope effect in the agricultural (32.8 ± 1.4‰) and meadow (28.4 ± 2.1‰) soils, whereas the isotope effect for the coupled net mineralization and nitrification was small in the forest and riparian soils (Table 1). Significant NO_3^- consumption (0.75 ± 0.02 to 5.45 ± 0.67 μg N·g^{-1}·d^{-1}) relative to the gross nitrification were indicated in the meadow, forest, and riparian soils (Table 1). The ratio of gross NO_3^- consumption to gross nitrification ranged between 0.44 and 0.53 (Table 1). Only NO_3^- consumption in the meadow soil, however, was associated with an appreciable N isotope effect (8.1 ± 4.9‰) (Table 1).

3.2. Field snowmelt sampling

The snow water samples had a NO_3^- concentration of 0.26 ± 0.04 mg N·L^{-1} and a Δ^{17}O of 25.1 ± 0.1‰. The snowmelt event captured in this study introduced snow NO_3^- into the surface soil, leading to nonzero Δ^{17}O-NO_3^- values for the first (2.1 ± 1.5‰) and second (1.9 ± 1.3‰) days of soil sampling (Fig. 5c), although

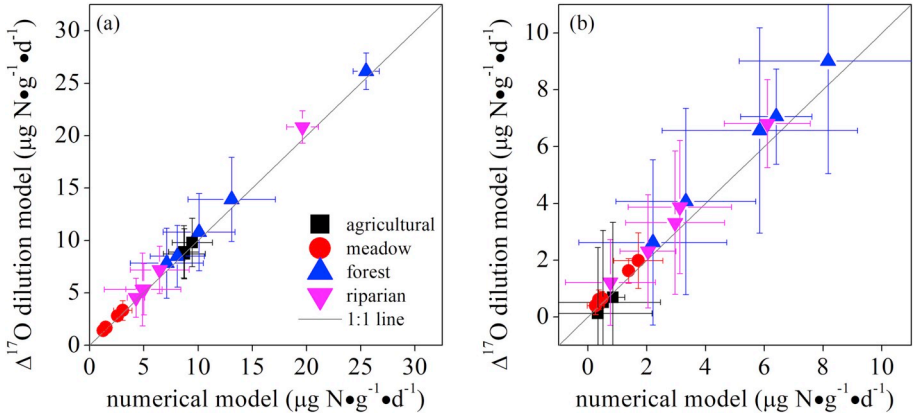

Fig. 4. Gross nitrification (a) and NO_3^- consumption (b) rates estimated using the numerical model and the Δ^{17}O dilution model for every two consecutive soil samplings in the laboratory incubation experiments. The error bars denote the 95% confidence intervals of the estimated rates.

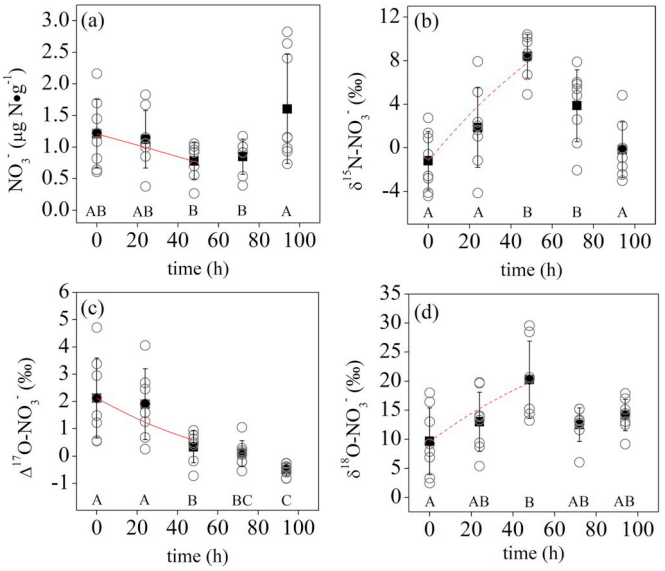

Fig. 5. Measured (symbols) and modeled (solid and dashed lines) concentrations and isotopic composition of NO_3^- from the field sampling following the snowmelt. Mean and standard deviation (solid black squares and error bars) are calculated based on eight replicate measurements (open gray cycles). The letters below the symbols denote significant differences determined by one-way ANOVA with a pairwise Bonferroni test ($P < 0.05$).

large deviations were observed in the replicate measurements (n = 8) probably due to soil heterogeneity. A significant decline in the $\Delta^{17}O\text{-}NO_3^-$ occurred between day 2 and day 3 such that the $\Delta^{17}O\text{-}NO_3^-$ values measured for the last three days of sampling were not significantly different from zero (Fig. 5c; $P > 0.05$). Post-snowmelt variations in the soil NO_3^- concentration and the dual NO_3^- isotopes were more complex. The NO_3^- concentration appeared to be significantly increased on day 5 (Fig. 5a), while both $\delta^{15}N\text{-}NO_3^-$ and $\delta^{18}O\text{-}NO_3^-$ increased significantly from day 1 through day 3 and then decreased toward day 5 (Fig. 5b and d). The $\Delta^{17}O\text{-}NO_3^-$ was significantly and negatively correlated with the $\delta^{15}N\text{-}NO_3^-$ if only data measured in the first three sampling days was used in the linear regression (Fig. 6a). A negative, albeit not statistically significant (P = 0.051), association was also found between the $\Delta^{17}O\text{-}NO_3^-$ and the $\delta^{18}O\text{-}NO_3^-$ for the first three sampling days (Fig. 6a). Significant and negative correlations were also detected between the $\delta^{15}N\text{-}NO_3^-$ and the natural logarithm of the NO_3^- concentration (Fig. 6b). When plotting the $\delta^{15}N\text{-}NO_3^-$ and the $\delta^{18}O\text{-}NO_3^-$ together, a significant linear relationship with a slope of 0.63 emerged for the entire sampling period (Fig. 6c). The linear regression fit was improved and the slope of the regression line was increased to 0.89 if only data measured in the first three sampling days was included (Fig. 6c). The numerical model was used to fit the NO_3^- concentration and $\Delta^{17}O\text{-}NO_3^-$ for the first three sampling days when nonzero $\Delta^{17}O\text{-}NO_3^-$ was generally measurable (Fig. 5c) and found that gross nitrification and NO_3^- consumption rates were 1.3 ± 2.1 μg $N{\cdot}g^{-1}{\cdot}d^{-1}$ and 1.7 ± 2.1 μg $N{\cdot}g^{-1}{\cdot}d^{-1}$, respectively.

4. Discussion

4.1. $\Delta^{17}O\text{-}NO_3^-$ as a conservative tracer of gross soil nitrification and nitrate consumption

The numerical model that explicitly simulates the O isotopologue pools of NO_3^- at the process-level provides a benchmark for examining the conservative nature of $\Delta^{17}O\text{-}NO_3^-$ during soil nitrification and NO_3^- consumption. Based on the numerical model, a wide range of gross nitrification and NO_3^- consumption rates was estimated using every two consecutive soil samplings for the four soils (Fig. 4; Table S2). The sensitivity of the estimated gross nitrification and NO_3^- consumption rates to β and magnitude of the O isotopic fractionations (1 σ) was on average 2.6 ± 1.5% and 6.0 ± 2.0%, respectively, for the four soils (Figs. S2–S5), which were much lower than the average margin of error (95% confidence level) of the estimated gross nitrification (20.2 ± 12.0%) and NO_3^- consumption (38.4 ± 16.7%) rates

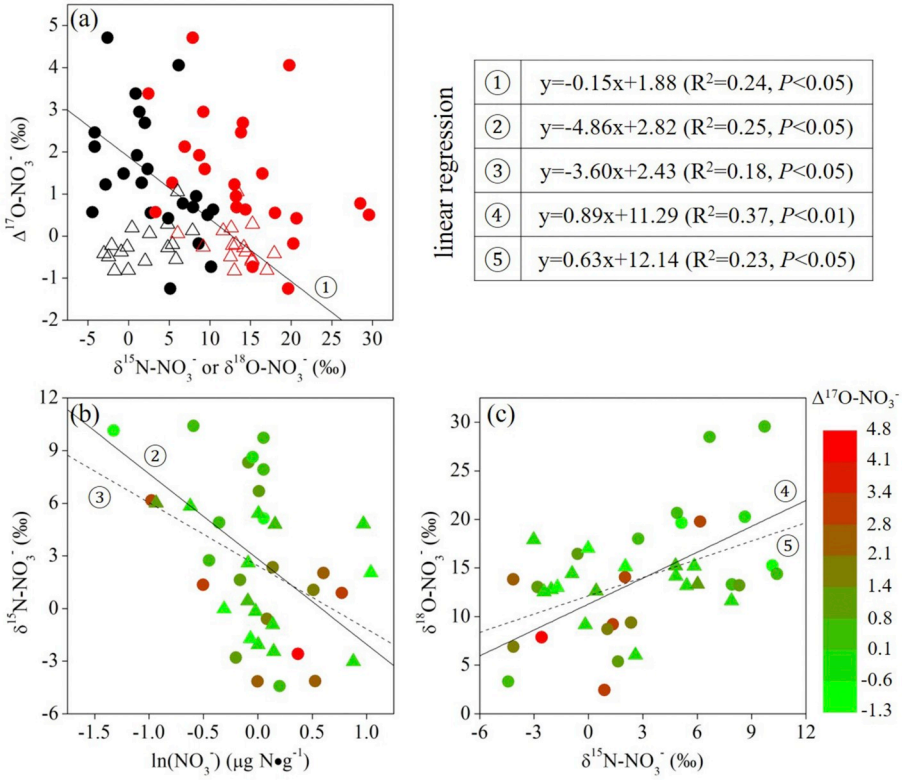

Fig. 6. Relationships among soil NO_3^- concentration and the triple NO_3^- isotopes in the field soil sampling following the snowmelt. (a) Relationships between $\Delta^{17}O\text{-}NO_3^-$ and $\delta^{15}N\text{-}NO_3^-$ (black symbols) and between $\Delta^{17}O\text{-}NO_3^-$ and $\delta^{18}O\text{-}NO_3^-$ (red symbols). (b) Relationship between $\delta^{15}N\text{-}NO_3^-$ and the natural logarithm of soil NO_3^- concentration in association with $\Delta^{17}O\text{-}NO_3^-$ (color scale). (c) Relationship between $\delta^{15}N\text{-}NO_3^-$ and $\delta^{18}O\text{-}NO_3^-$ in association with $\Delta^{17}O\text{-}NO_3^-$ (color scale). In all the panels, data measured for day 1 through day 3 and for day 4 through day 5 are shown as cycles and triangles, respectively. The solid and dashed lines represent linear regression fits for the first three sampling days and the entire sampling duration, respectively. The linear regression fits are labeled and corresponding to the regression equations shown in the inserted table. (For interpretation of the references to color in this figure legend, the reader is referred to the Web version of this article.)

propagated from the analytical and experimental errors (Fig. 4; Table S2). Therefore, the results from the sensitivity test corroborate the conservative nature of $\Delta^{17}O\text{-}NO_3^-$ and suggest that although $\delta^{18}O$ and $\delta^{17}O$ of NO_3^- are controlled by the O isotopic fractionations and their respective β values during nitrification and NO_3^- consumption, no precise knowledge of these controlling factors need be known to apply $\Delta^{17}O\text{-}NO_3^-$ for estimating gross nitrification and NO_3^- consumption rates using the numerical model, even though the $\Delta^{17}O$ calculations are made relative to $\delta^{18}O$ and $\delta^{17}O$ values.

Importantly, when the numerical model was applied to every two consecutive soil samplings, the large uncertainties in the estimated rates, especially the gross NO_3^- consumption rates (Fig. 4), indicate a high method detection limit at this fine temporal resolution. It is well recognized in ^{15}N tracer-based studies that gross rate estimates are most reliable when N transformations are relatively fast so that the tracer pool is significantly diluted within measurement intervals (Davidson et al., 1991; Hart et al., 1994; Smith et al., 1994). In our case, decline of the $\Delta^{17}O\text{-}NO_3^-$ ranged from 0.21‰ to 1.28‰ between every two consecutive samplings for the four soils (Fig. 2e) and was generally modest relative to the precision of the replicate $\Delta^{17}O\text{-}NO_3^-$ measurements (i.e., ± 0.13‰). If the gross nitrification and NO_3^- consumption rates are estimated for the entire incubation duration using soil extractions at the beginning and end of each incubation experiment, the average errors in the gross nitrification and NO_3^- consumption rates are significantly reduced to 5.1 ± 2.5% and 11.4 ± 5.2%, respectively, for the four soils (Fig. S6). This indicates that error propagation in estimating the gross nitrification and NO_3^- consumption rates is a signal-to-noise problem in nature (Davidson et al., 1991). It is therefore not surprising to see that the gross NO_3^- consumption rates, which were significantly lower than the gross nitrification rates in this study, had larger relative errors. From this perspective, the proposed $\Delta^{17}O$-based rate estimation may have a higher limit of detection than other methods based on highly enriched ^{15}N tracers (e.g., 99% $^{15}NO_3^-$). Consequently, temporal resolution is an important factor that needs to be considered and tested when applying the proposed $\Delta^{17}O$-based numerical model for rate estimation. Given the high temporal sensitivity of the precision of the rate estimates, fitting the numerical model to multiple observations made over each incubation is required for deriving precise gross N transformation rates for the studied soils (see below).

Compared to the numerical model, the $\Delta^{17}O$ dilution model tended to overestimate gross nitrification (7.0 ± 3.6%) and NO_3^- consumption (17.1 ± 10.8%) rates at the fine temporal resolution (i.e., every two consecutive samplings; Fig. 4; Table S2). This overestimation is reduced to 3.6 ± 0.8% and 7.7 ± 1.6% for gross nitrification and NO_3^- consumption rates, respectively, when soil extractions at the beginning and end of each soil incubation were used for the rate estimation (Fig. S6). The differences between the rates estimated using the two models are probably due to slight violations of the assumptions inherent to the isotope dilution concept as a consequence of the variability of β in characterizing the mass-dependent fractionations during multi-step fractionation processes (Miller, 2002; Young et al., 2002) and the nonlinear mixing behavior of $\Delta^{17}O$ defined using Equation (4) (Kaiser et al., 2004; Luz and Barkan, 2005). However, these differences are generally within the margin of error of the respective estimates at both fine and coarse temporal resolutions (Fig. 4; Fig. S6), indicating that application of the $\Delta^{17}O$ dilution model will lead to acceptable levels of uncertainty under analytical and experimental conditions similar to those documented in this study. Therefore, the comparison between the two models provides evidence supporting the practical use of $\Delta^{17}O\text{-}NO_3^-$ in the isotope dilution model, even though it may not strictly meet the assumptions inherent to the isotope dilution concept. Future studies should directly compare the $\Delta^{17}O$ dilution model with the established $^{15}NO_3^-$ tracer-based approaches to further evaluate its applicability under a wider range of soil conditions.

4.2. $\Delta^{17}O\text{-}NO_3^-$ as a bridge between soil NO_3^- cycling rates and isotopic fractionations

Robust rate estimation was achieved by fitting the numerical model to all observations made over each soil incubation (except the first data point for the forest and riparian soils; Table 1). The good agreement between the observed and simulated results indicates that gross nitrification and NO_3^- consumption followed zero-order kinetics throughout the short-term incubation experiments in the four soils (Fig. 2). While zero-order kinetics might be favored by the high N availability in the agricultural soil (Shi and Norton, 2000), the constant rates of nitrification and NO_3^- consumption in the three non-agricultural soils suggest that the NO_3^- dynamics might be coupled with C transformations, which operated through much larger pool sizes (Myrold and Tiedje, 1986; Mary et al., 1998). The estimated gross nitrification and NO_3^- consumption rates for the four soils are well within the range of values reported in a meta-analysis of ^{15}N tracer-based gross nitrification and NO_3^- consumption rates for woodland, grassland, and agricultural soils (Booth et al., 2005) (Table 1). The estimated gross nitrification rates also followed the same trend as the nitrification potential, an index of autotrophic nitrifier abundance, suggesting the high consistency of our $\Delta^{17}O$-based modeling approach. Furthermore, while the estimated gross NO_3^- consumption was significantly lower than the gross nitrification rate in the agricultural soil (Table 1), the estimated ratio of gross NO_3^- consumption to gross nitrification for the three non-agricultural soils (0.44–0.53) is generally consistent with the average ratio (0.59) found for a wide variety of natural soils in ^{15}N tracer-based studies (Booth et al., 2005) and the established paradigm that NO_3^- consumption is positively correlated with nitrification in unmanaged soils (Booth et al., 2005).

In addition to revealing NO_3^- cycling rates, tracing soil nitrification and NO_3^- consumption using $\Delta^{17}O\text{-}NO_3^-$ provides a unique opportunity to couple NO_3^- transformation with dynamics of the dual NO_3^- isotopes, which cannot be achieved using the ^{15}N tracer-based techniques. During the incubations, $\Delta^{17}O\text{-}NO_3^-$ values varied linearly with $\delta^{15}N\text{-}NO_3^-$ values in the four soils (Fig. 3a). Since $\Delta^{17}O\text{-}NO_3^-$ behaves closely as a conservative tracer during nitrification and NO_3^- consumption as discussed above, we interpret the observed linear covariation between $\Delta^{17}O\text{-}NO_3^-$ and $\delta^{15}N\text{-}NO_3^-$ to have arisen from a two-component mixing between the standing pool of NO_3^- with a nonzero $\Delta^{17}O\text{-}NO_3^-$ originating from the Chilean NO_3^- fertilizer and a microbial source of NO_3^- that has $\Delta^{17}O = 0$ and appeared to be variable in $\delta^{15}N$ among the four soils. The $\delta^{15}N$ of this microbially-mediated NO_3^- ($\delta^{15}N_M$) can be estimated by extrapolating the linear regression of $\Delta^{17}O\text{-}NO_3^-$ and $\delta^{15}N\text{-}NO_3^-$ to the x axis (i.e., the x-intercept) where $\Delta^{17}O = 0$ (Fig. 3a). The values of $\delta^{15}N_M$ obtained in this way were −29.2 ± 2.4‰, −12.8 ± 1.1‰, 2.3 ± 0.2‰, and 2.4 ± 0.1‰ for the agricultural, meadow, forest, and riparian soils, respectively (errors are given as one standard deviation of the x-intercept) (Fig. 3a).

To investigate how $\delta^{15}N_M$ is controlled by nitrification and NO_3^- consumption, a forward modeling of the numerical model was conducted by varying the key parameters in the model (i.e., N transformation rates and N isotope effects) and simultaneously tracking their covariations with $\delta^{15}N_M$. The results confirmed the linear relationship between $\Delta^{17}O\text{-}NO_3^-$ and $\delta^{15}N\text{-}NO_3^-$ under various simulated conditions of nitrification and NO_3^- consumption (Fig. 7) and revealed that the variations in $\delta^{15}N_M$ can be explained by a steady state isotope model:

$$\delta^{15}N_M = \delta^{15}N_N + \frac{R_{NC}}{R_N} * {}^{15}\varepsilon_{NC} \quad (7)$$

where $\delta^{15}N_N$ is the $\delta^{15}N$ end-member of nitrification-produced NO_3^- and $^{15}\varepsilon_{NC}$ is the N isotope effect for NO_3^- consumption. Since $\delta^{15}N_N$ can be estimated from the $\delta^{15}N$ of nitrification substrate ($\delta^{15}N_S$) and the N isotope effect associated with nitrification ($^{15}\varepsilon_N$), equation (7) can be rewritten as:

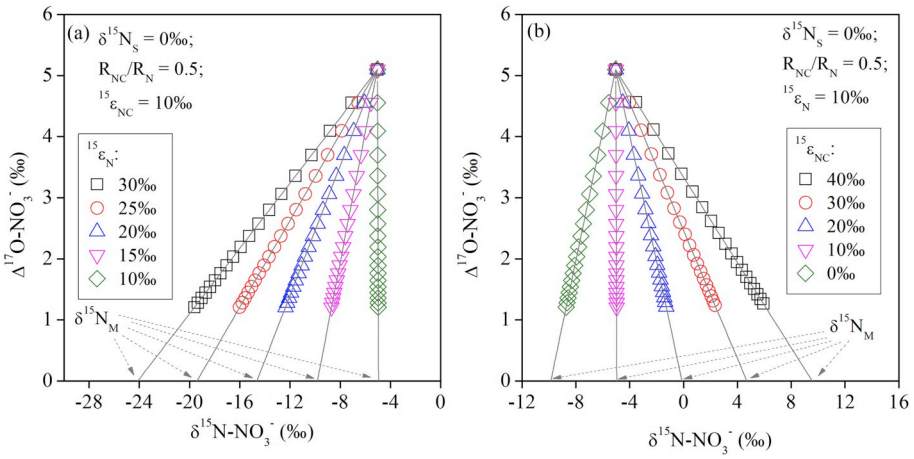

Fig. 7. Forward analysis of the numerical model showing evolution of $\Delta^{17}O\text{-}NO_3^-$ and $\delta^{15}N\text{-}NO_3^-$ values during simulated nitrification and NO_3^- consumption. In the forward modeling, either $^{15}\varepsilon_N$ (a) or $^{15}\varepsilon_{NC}$ (b) was varied within range shown in the legends while holding $\delta^{15}N_S$, R_N, and R_{NC} constant in the model. Parameter values used in the forward modeling are: R_{NC}/R_N = 0.5, $\delta^{15}N_S$ = 0‰, and initial $\Delta^{17}O\text{-}NO_3^-$ = 5‰. The gray lines are linear regression fits of $\Delta^{17}O\text{-}NO_3^-$ and $\delta^{15}N\text{-}NO_3^-$ with the x intercept denoting $\delta^{15}N_M$.

$$\delta^{15}N_M = (\delta^{15}N_S - {}^{15}\varepsilon_{NC}) + \frac{R_{NC}}{R_N} * {}^{15}\varepsilon_{NC} \quad (8)$$

An illustration of the pattern underlying Equation (8) is shown in Fig. 7 by varying either $^{15}\varepsilon_N$ or $^{15}\varepsilon_{NC}$ while holding the other parameters constant in the numerical model. According to Equation (8) and Fig. 7, the sign and magnitude of the linear regression of $\Delta^{17}O\text{-}NO_3^-$ and $\delta^{15}N\text{-}NO_3^-$ depends on the difference between $\delta^{15}N_M$ and the initial $\delta^{15}N$ of the standing NO_3^- pool and is ultimately controlled by the difference between $^{15}\varepsilon_N$ and $^{15}\varepsilon_{NC}$ given constant $\delta^{15}N_S$, R_N, and R_{NC} (Fig. 7).

The distinct $\delta^{15}N_M$ values revealed for the four soils are in accordance with the estimated $^{15}\varepsilon_N$ and $^{15}\varepsilon_{NC}$ using the numerical model and are reflective of the relationships between the gross NO_3^- cycling rates and soil properties. Large $^{15}\varepsilon_N$ (32.8 ± 1.4‰) was estimated for the agricultural soil where gross nitrification was directly stimulated by the NH_4^+ fertilization (Fig. 2; Table 1). The large $^{15}\varepsilon_N$ resulted in the low $\delta^{15}N_N$ and $\delta^{15}N_M$, driving the positive relationship between the $\Delta^{17}O\text{-}NO_3^-$ and the $\delta^{15}N\text{-}NO_3^-$ (Fig. 3a). The estimated $^{15}\varepsilon_N$ was highly consistent with results from culture studies using ammonia-oxidizing bacteria and archaea under optimum substrate conditions (e.g., 25‰–35‰) (Mariotti et al., 1981; Casciotti et al., 2003), highlighting the fully expressed isotope effect of nitrification in NH_4^+-rich soils (Mariotti et al., 1981). It is important to note that since $^{15}\varepsilon_N$ is estimated using both $\delta^{15}N\text{-}NO_3^-$ and $\delta^{15}N\text{-}NH_4^+$ values and is constrained by the $\Delta^{17}O$-derived rate estimates in the numerical model, any deviation from complete mass balance between NH_4^+ and NO_3^- due to concurrent net mineralization and/or NO_3^- consumption is accounted for in the estimate of $^{15}\varepsilon_N$ (Casciotti et al., 2003). Gross NO_3^- consumption in the agricultural soil was very low and associated with a $^{15}\varepsilon_{NC}$ not significantly different from zero (Table 1), reflecting the low microbial NO_3^- demand imposed by the C limitation (Shi and Norton, 2000; Cheng et al., 2017).

In contrast to the agricultural soils, small and positive $\delta^{15}N_M$ values were estimated for the forest and riparian soils (Fig. 3a), consistent with the expectation that the isotope effect for nitrification is under-expressed under NH_4^+-limiting conditions (Mariotti et al., 1981). The positive $\delta^{15}N_M$ values in conjunction with the high gross nitrification rates in these two soils are evidence that nitrifiers were likely living in close-enough association with mineralizers to immediately deplete available NH_4^+ (Inselsbacher et al., 2013). Although we were not able to derive estimates for microbial NH_4^+ assimilation using the $\Delta^{17}O$-based numerical model, there is evidence that autotrophic nitrifiers are able to compete with heterotrophs for NH_4^+ in soils with high overall N availability, shifting the cycling of inorganic N to be NO_3^--dominated (Corre et al., 2002; Schimel and Bennett, 2004). A large and active autotrophic nitrifier community was also confirmed by the measured high nitrification potential in these two soils (Table 1). Moreover, the NO_3^- production and accumulation in the forest and riparian soils might also be partially contributed by heterotrophic nitrification, where organic N and NH_4^+ is converted to NO_2^- or NO_3^- by a diverse group of organisms (Müller et al., 2004). Since heterotrophic nitrifiers can utilize both organic N and NH_4^+, they were found to account for an increased proportion of nitrification rates at low pH, especially in soils containing low C:N organic matter (Booth et al., 2005; Müller et al., 2004; Inselsbacher et al., 2013). Essentially, the estimated small $^{15}\varepsilon_N$ for the forest and riparian soils are in line with the minor isotopic fractionation during mineralization (i.e., < 2‰) documented in previous studies (Denk et al., 2017), and highlight the direct connection between the organic N and NO_3^- pools. On the other hand, gross NO_3^- consumption was associated with a negligible $^{15}\varepsilon_{NC}$ in these two soils (Table 1), suggesting that the NO_3^- was dominantly consumed via microbial assimilation (Fig. 1) (Denk et al., 2017). Substantial NO_3^- assimilation has long been reported in grassland and forest soils (Schimel et al., 1989; Davidson et al., 1991; Stark and Hart, 1997). Microbial NO_3^- assimilation as the dominant NO_3^- sink in the forest and riparian soils is congruent with the greater availability of organic C and the depleted NH_4^+ pool that might have promoted microbial demand for NO_3^- and rapid NO_3^- recycling in these two soils (Davidson et al., 1991; Inselsbacher et al., 2013; Cheng et al., 2017).

Both gross nitrification and NO_3^- consumption were associated with a significant isotope effect in the meadow soil (i.e., 28.4 ± 2.1‰ and 8.1 ± 4.9‰, respectively) (Table 1), resulting in a negative $\delta^{15}N_M$ and a positive relationship between $\Delta^{17}O\text{-}NO_3^-$ and $\delta^{15}N\text{-}NO_3^-$ (Fig. 3a). The large $^{15}\varepsilon_N$ is consistent with the theoretical consideration that full expression of the kinetic isotope effect of nitrification is favored under conditions of high NH_4^+ availability but low nitrification rates (Mariotti et al., 1981; Maggi et al., 2008). Compared to the forest and riparian soil, the low nitrification potential of the meadow soil indicates a small population of autotrophic nitrifiers (Table 1) (Davidson et al., 1991). It is possible that nitrifiers were out-competed by heterotrophs for available NH_4^+ in the meadow soil, as previously observed for NH_4^+-rich soils with overall modest N availability (Schimel and Bennett, 2004). The tight cycling of N between the organic N and NH_4^+ pools seems to be supported by significant net mineralization (Table 1) and the generally elevated $\delta^{15}N\text{-}NH_4^+$ values (Fig. 2b), although firm conclusions cannot be drawn without further constraints on gross mineralization and NH_4^+ assimilation. Unlike the other three soils, the significant $^{15}\varepsilon_{NC}$ in the meadow soil implies the occurrence of denitrification as an important NO_3^- sink in the meadow soil. The hypothesis that denitrification was active is supported by the higher clay content that might favor formation of anaerobic microsites even in sieved, well-mixed soils (Keiluweit et al., 2018) and the presence of denitrifying bacteria as revealed in the denitrification potential assay (Table 1). Moreover, high NH_4^+ concentrations in the meadow soil

could inhibit microbial assimilation of NO_3^- (Rice and Tiedje, 1989; Mary et al., 1998) and therefore increase the relative importance of NO_3^- consumption via denitrification. Unfortunately, there are currently large uncertainties in the isotope effects for microbial NO_3^- assimilation and denitrification measured in culture- and soil-based studies (Fig. 1) (Denk et al., 2017), preventing quantitative partitioning of the respective pathways using the estimated $^{15}\varepsilon_{NC}$. However, knowing $^{15}\varepsilon_{NC}$ itself is important and suffices for setting the stage for further investigation into the NO_3^- consumption pathways.

From the above discussion, we conclude that the coupled measurement and numerical modeling of $\Delta^{17}O\text{-}NO_3^-$ and $\delta^{15}N\text{-}NO_3^-$ can bridge soil NO_3^- cycling rates with isotopic fractionations and help explain mechanisms causing variations in gross nitrification and NO_3^- consumption. The clear differences among the studied four soils in terms of gross N rates and N isotope effects highlight the proximate control of the soil microbial community structure on soil NO_3^- cycling. Soil microbial activity is in turn strongly affected by a wide range of physical and chemical factors, such as soil texture, soil organic C, and availability of N sources for microbial use. While kinetic isotope effects are a fundamental parameter to probe microbial activity underlying soil N transformations (Mariotti et al., 1981), it is often the case that an effect demonstrated clearly in culture studies is more equivocal in a complex soil environment (Maggi et al., 2008). Our $\Delta^{17}O$-based modeling approach capable of deriving gross N rates and N isotope effects simultaneously is therefore an effective way to reduce ambiguities in the N isotope systematics of soil NO_3^- cycling and to help constrain the $\delta^{15}N$ end-member of nitrification-produced NO_3^-, which is notoriously hard to predict in dual isotope-based ecosystem models (Hall et al., 2016). On the other hand, as the first attempt to use $\Delta^{17}O\text{-}NO_3^-$ as a tracer of soil NO_3^- cycling, we focused on nitrification and NO_3- consumption and followed the established notion in soil ^{15}N tracer studies to make the numerical model as simple as possible (Mary et al., 1998; Müller et al., 2004). Future work could extend the numerical model to include further realistic N transformation pathways (e.g., gross mineralization and NH_4^+ assimilation) and associated isotope effects (Denk et al., 2017). Moreover, because N assimilation is an input rate for only a part of the organic N pool which is itself a small proportion of the total soil N (Myrold and Tiedje, 1986; Smith et al., 1994), a robust estimate of the active organic N pool size and its $\delta^{15}N$ should be of primary importance for future application of the numerical model.

Finally, as revealed by a series of forward modeling analyses focusing on the linear correlations between $\Delta^{17}O\text{-}NO_3^-$ and $\delta^{18}O\text{-}NO_3^-$ (Fig. 3b), Equation (7) is equally applicable to deriving the $\delta^{18}O$ end-member of nitrification-produced NO_3^- ($\delta^{18}O_N$) (results not shown). In this case, $\delta^{18}O_N$ is collectively controlled by the $\delta^{18}O$ of the substrates (O_2 and H_2O), the O isotope effects associated with the O atom incorporation, and the extent to which the O is exchanged between NO_2^- and H_2O (Casciotti et al., 2010; Buchwald and Casciotti, 2010). However, as the NO_3^- consumption processes did not fractionate the NO_3^- isotopes significantly in the agricultural, forest, and riparian soils, the $\delta^{18}O_N$ can be approximated by the x intercept of the linear regression of $\Delta^{17}O\text{-}NO_3^-$ and $\delta^{18}O\text{-}NO_3^-$ (i.e., $\delta^{18}O_M$) for these three soils. The estimated $\delta^{18}O_N$ ranged from -7.0 ± 0.6‰ to -0.9 ± 0.3‰ (Fig. 3b). Although we did not have constraints on the factors controlling the $\delta^{18}O_N$ except the $\delta^{18}O$ value of the added Milli-Q water (-10.1‰), the estimated $\delta^{18}O_N$ values intersect the range of $\delta^{18}O_N$ reported for temperate forest soils (e.g., -4‰–15‰; Fang et al. (2012)). Nevertheless, in previous studies $\delta^{18}O_N$ was routinely estimated from an isotopic mass balance based on the net accumulation of NO_3^- during aerobic soil incubations. Using the $\Delta^{17}O$-based modeling approach, we show that substantial NO_3^- consumption can occur under aerobic soil conditions. It is not clear how the reported $\delta^{18}O_N$ in the literature was affected by failure to account for potential NO_3^- consumption in the mass balance calculation. We argue that the coupled measurement and modeling of $\Delta^{17}O\text{-}NO_3^-$ and $\delta^{18}O\text{-}NO_3^-$ is a superior approach to derive unbiased estimates of $\delta^{18}O_N$, which are critical for its quantitative use in tracing sources and fate of NO_3^- in terrestrial and aquatic ecosystems.

4.3. Post-snowmelt soil NO_3^- dynamics and implications for modeling denitrification using the dual NO_3^- isotopes

The $\Delta^{17}O\text{-}NO_3^-$ values from the field soil cores are consistent with the results from synoptic or precipitation event-based surface soil sampling in temperate and semiarid ecosystems (e.g., 0‰–4‰) (Fig. 5c) (Michalski et al., 2004; Costa et al., 2011; Fang et al., 2015). Based on the $\Delta^{17}O\text{-}NO_3^-$ of snow water (25.1 ± 0.1‰), a simple mixing calculation indicates that snow NO_3^- accounted for 8.2% and 7.4% of the surface soil NO_3^- pool on the first two sampling days, respectively, in line with the finding by Costa et al. (2011) that rainwater NO_3^- contributed 7% of surface soil NO_3^- immediately after a rain event in a temperate forest in Michigan, USA. A significant decline in the $\Delta^{17}O\text{-}NO_3^-$ was observed between day 2 and day 3 with no concomitant change in the NO_3^- concentration during the first three days of sampling (Fig. 5a and c), indicating cycling of NO_3^- via nitrification and NO_3^- consumption following the snowmelt. The co-occurring nitrification and NO_3^- consumption during the first three sampling days were also supported by rate estimates from the numerical model (1.3 ± 2.1 and 1.7 ± 2.1 $\mu g\, N \cdot g^{-1} \cdot d^{-1}$, respectively) (Fig. 5a and b). However, these rate estimates have large uncertainties propagated from the large deviations in the replicate NO_3^- concentration and $\Delta^{17}O\text{-}NO_3^-$ measurements (Fig. 5a and c). This reinforces the notion that for any isotope-based N tracing models, the accuracy of the model estimates strongly depends on the data quality (Inselsbacher et al., 2013). Further, it highlights the difficulty in using precipitation $\Delta^{17}O\text{-}NO_3^-$ as a natural tracer of nitrification and NO_3^- consumption in undisturbed soils where factors like root density and presence of soil microsites can lead to significant spatial heterogeneity. From this perspective, application of the label injection protocol that is commonly used in the ^{15}N tracer studies (Davidson et al., 1991) is a logical next step for testing the usefulness of $\Delta^{17}O\text{-}NO_3^-$ under field conditions.

Despite the large uncertainties in the rate estimates, pooling the measurements over the first three sampling days provides multiple lines of evidence suggesting that denitrification was an important NO_3^- consumption pathway following the snowmelt. The $\delta^{15}N\text{-}NO_3^-$ in the surface soil displayed a significant relationship of ^{15}N enrichment with the logarithm of the NO_3^- concentration (Fig. 6b). The slope of this relationship identifies an apparent isotope effect of 4.9‰ for the NO_3^- consumption, approximating denitrification of a quasi-closed NO_3^- pool (Yu et al., 2016). Moreover, the increase in the $\delta^{15}N\text{-}NO_3^-$ was linked to the $\delta^{18}O\text{-}NO_3^-$ (Fig. 5b and d) as manifested in the linear relationship with a slope of 0.89 (Fig. 6c), characteristic of denitrification activity (Groffman et al., 2006). Finally, the negative correlation between the $\Delta^{17}O\text{-}NO_3^-$ and the $\delta^{15}N\text{-}NO_3^-$ suggests a positive $\delta^{15}N_M$ which is indicative of denitrification that has a significant isotope effect (Figs. 6a and 7b). Indeed, the importance of denitrification in cold soils during snowmelt has been reported in temperate ecosystems where snowmelt often represents a period of soil saturation (Fig. S1) and potential NO_3^- loss (Hall et al., 2016). Using direct N_2 flux measurement in a northern upland forest, Morse et al. (2015) revealed a burst of denitrification activity in apparently oxic surface soils during snowmelt, which was triggered by increased soil water content and N supply from mineralization and nitrification.

Thus, using the triple NO_3^- isotopes, we provide direct evidence for the co-occurrence of nitrification and denitrification in surface soils, which has important implications for modeling denitrification using dual NO_3^- isotopes. Because the dilution of $\Delta^{17}O\text{-}NO_3^-$ over space and time is exclusively driven by nitrification, the co-occurrence of nitrification and denitrification is best illustrated by a triple isotope plot of NO_3^- (Fig. 6). As shown in Fig. 6, isotope enrichment diagnostic of denitrification was paralleled by nitrification. Because nitrification has opposite effects on $\delta^{15}N\text{-}NO_3^-$ and $\delta^{18}O\text{-}NO_3^-$ as revealed in the laboratory incubation of the meadow soil, co-occurring nitrification may

obscure isotopic signatures from denitrification, complicating the interpretation of the dual NO_3^- isotopes beyond the unidirectional NO_3^- consumption. To investigate how the identification of denitrification can be affected by the co-occurring nitrification, we ran the numerical model to fit the observed $\delta^{15}N\text{-}NO_3^-$ and $\delta^{18}O\text{-}NO_3^-$ values based on the estimated gross nitrification and NO_3^- consumption rates. Although soil NH_4^+ concentration and $\delta^{15}N\text{-}NH_4^+$ were not measured for the field samples, excess NH_4^+ relative to NO_3^- was observed on an annual basis at this site (Yu and Elliott, unpublished data), suggesting that the isotope effect associated with nitrification was likely expressed following the snowmelt. Therefore, the $\delta^{15}N$ and $\delta^{18}O$ of nitrification-produced NO_3^- were assumed to be −12.8‰ and −0.5‰, respectively, in the model, consistent with the $\delta^{15}N_M$ and $\delta^{18}O_M$ measured for the meadow soil in the incubation experiment. The results show that the observed variations in $\delta^{15}N\text{-}NO_3^-$ and $\delta^{18}O\text{-}NO_3^-$ during the first three sampling days can be possibly explained by an isotope effect of 18‰ for both enrichments of $\delta^{15}N\text{-}NO_3^-$ and $\delta^{18}O\text{-}NO_3^-$ (Fig. 5b and d). This potentially large isotope effect for both N and O isotopic fractionations would have been obscured, if we had assessed relationships among concentration and the dual isotopes of NO_3^- without the context of the co-occurring nitrification. The isotopic imprints of denitrification would have been further obscured, if the dual NO_3^- isotopes measured in the last two sampling days had been misrepresented in the analysis of denitrification, leading to lower apparent isotope effect (3.6‰) (Fig. 6b) and a slope of the $\delta^{15}N\text{-}NO_3^-$ versus $\delta^{18}O\text{-}NO_3^-$ trajectory significantly lower than 1 (Fig. 6c).

These modeling exercises highlight the competing fractionation from nitrification and denitrification in redox-heterogeneous environment (e.g., surface soil horizon) that may explain the long-lasting discrepancies between field- and laboratory-derived isotope systematics of denitrification (Granger and Wankel, 2016). In previous studies, the apparent isotope effects for denitrification derived from field observations in wet soils and freshwater systems are often lower than 10‰ (Mariotti et al., 1988; Osaka et al., 2010; Yu et al., 2016) and also lower than those reported in laboratory experiments with denitrifying bacteria and anaerobically incubated soil samples (Fig. 1) (Mariotti et al., 1981; Granger et al., 2008; Denk et al., 2017). Moreover, the $\delta^{15}N\text{-}NO_3^-$ versus $\delta^{18}O\text{-}NO_3^-$ trajectory inferred from field-observed denitrification events are variable, with the slope ranging widely from 0.5 to 2 (Groffman et al., 2006), while a slope of ~1 was clearly demonstrated for denitrifying bacteria (Granger et al., 2008). Based on the above discussion, we conclude that when combined with constraints from controlled laboratory experiments, the coupled measurement and modeling of triple NO_3^- isotopes has the potential to disentangle the isotopic overprinting from nitrification and denitrification in soils, allowing for a more robust interpretation of denitrification in dual NO_3^- isotope space.

5. Conclusions

While $\Delta^{17}O$ has been increasingly used to examine atmospheric NO_3^- deposition and its subsequent retention in terrestrial and aquatic ecosystems, few studies have explored the quantitative use of $\Delta^{17}O$ in probing gross nitrification and NO_3^- consumption in soils. In this proof-of-concept study, we investigated the robustness of $\Delta^{17}O\text{-}NO_3^-$ as a tracer of nitrification and NO_3^- consumption through developing and validating a $\Delta^{17}O$-based numerical model. The results confirmed the conservative nature of $\Delta^{17}O\text{-}NO_3^-$ and highlighted the mechanistic coupling between $\Delta^{17}O\text{-}NO_3^-$ and the dual NO_3^- isotopes in characterizing isotope effects associated with nitrification and NO_3^- consumption. While care should be taken to apply $\Delta^{17}O\text{-}NO_3^-$ under field conditions where its tracing power may be compromised by soil heterogeneity, coupled measurement and modeling of the triple NO_3^- isotopes has great potential to discern and quantify isotopic overprinting from nitrification and denitrification in redox-dynamic soil horizons. Given that the initial isotopic composition of nitrification-produced NO_3^- and its subsequent enrichments over space and time are at the core of quantitative isotope models aiming to quantify denitrification at the watershed scale, the combined use of the triple NO_3^- isotopes in laboratory and field settings is expected to improve the performance of these models, and thus our broader understanding of denitrification. Finally, because denitrification obeys the mass-dependent fractionation law, N_2O, a potent greenhouse gas, produced from denitrification should inherit $\Delta^{17}O$ signal from $\Delta^{17}O$-labeled substrate NO_3^- and NO_2^-, while nitrification-produced N_2O should have $\Delta^{17}O \approx 0$. Hence, the potential for using $\Delta^{17}O$ to partition soil N_2O emission from nitrification and denitrification clearly merits exploration.

Acknowledgements

The authors thank Scott Wankel (WHOI) for generously providing the Chilean nitrate fertilizer, Dongqi Wang (East China Normal University) for help with soil characterization, Amy Townsend-Small (University of Cincinnati) for help with denitrification potential measurement, Duo Wu (Lanzhou University) for assistance during the field soil sampling, and Katherine Redling, Vivian Feng, Madeline Ellgass, and Madeline Gray (University of Pittsburgh) for assistance with the isotopic analyses. This work was supported by a National Science Foundation CAREER award (Grant No. 1253000) to E.M.E.

Appendix A. Supplementary data

Supplementary data to this article can be found online at https://doi.org/10.1016/j.soilbio.2018.09.029.

References

Belser, L.W., Mays, E.L., 1980. Specific inhibition of nitrite oxidation by chlorate and its use in assessing nitrification in soils and sediments. Applied and Environmental Microbiology 39 (3), 505–510.
Booth, M.S., Stark, J.M., Rastetter, E., 2005. Controls on nitrogen cycling in terrestrial ecosystems: a synthetic analysis of literature data. Ecological Monographs 75 (2), 139–157.
Buchwald, C., Casciotti, K.L., 2010. Oxygen isotopic fractionation and exchange during bacterial nitrite oxidation. Limnology & Oceanography 55 (3), 1064–1074.
Casciotti, K.L., Buchwald, C., McIlvin, M., 2013. Implications of nitrate and nitrite isotopic measurements for the mechanisms of nitrogen cycling in the Peru oxygen deficient zone. Deep Sea Research Part I: Oceanographic Research Papers 80, 78–93.
Casciotti, K.L., McIlvin, M., Buchwald, C., 2010. Oxygen isotopic exchange and fractionation during bacterial ammonia oxidation. Limnology & Oceanography 55 (2), 753–762.
Casciotti, K.L., Sigman, D.M., Hastings, M.G., Böhlke, J.K., Hilkert, A., 2002. Measurement of the oxygen isotopic composition of nitrate in seawater and freshwater using the denitrifier method. Analytical Chemistry 74 (19), 4905–4912.
Casciotti, K.L., Sigman, D.M., Ward, B.B., 2003. Linking diversity and stable isotope fractionation in ammonia-oxidizing bacteria. Geomicrobiology Journal 20 (4), 335–353.
Cheng, Y., Wang, J., Wang, J., Chang, S.X., Wang, S., 2017. The quality and quantity of exogenous organic carbon input control microbial NO_3^- immobilization: a meta-analysis. Soil Biology and Biochemistry 115, 357–363.
Corre, M.D., Schnabel, R.R., Stout, W.L., 2002. Spatial and seasonal variation of gross nitrogen transformations and microbial biomass in a Northeastern US grassland. Soil Biology and Biochemistry 34 (4), 445–457.
Costa, A.W., Michalski, G., Schauer, A.J., Alexander, B., Steig, E.J., Shepson, P.B., 2011. Analysis of atmospheric inputs of nitrate to a temperate forest ecosystem from $\Delta^{17}O$ isotope ratio measurements. Geophysical Research Letters 38 (15).
Davidson, E.A., Hart, S.C., Shanks, C.A., Firestone, M.K., 1991. Measuring gross nitrogen mineralization, and nitrification by ^{15}N isotopic pool dilution in intact soil cores. European Journal of Soil Science 42 (3), 335–349.
Decock, C., Six, J., 2013. An assessment of N-cycling and sources of N_2O during a simulated rain event using natural abundance ^{15}N. Agriculture, Ecosystems & Environment 165, 141–150.
Denk, T.R., Mohn, J., Decock, C., Lewicka-Szczebak, D., Harris, E., Butterbach-Bahl, K., Kiese, R., Wolf, B., 2017. The nitrogen cycle: a review of isotope effects and isotope modeling approaches. Soil Biology and Biochemistry 105, 121–137.
Fang, Y., Koba, K., Makabe, A., Takahashi, C., Zhu, W., Hayashi, T., Hokari, A.A., Urakawa, R., Bai, E., Houlton, B.Z., Xi, D., 2015. Microbial denitrification dominates nitrate losses from forest ecosystems. Proceedings of the National Academy of Sciences 112 (5), 1470–1474.
Fang, Y., Koba, K., Makabe, A., Zhu, F., Fan, S., Liu, X., Yoh, M., 2012. Low $\delta^{18}O$ values of nitrate produced from nitrification in temperate forest soils. Environmental Science &

Technology 46 (16), 8723–8730.
Felix, D.J., Elliott, E.M., Gish, T.J., McConnell, L.L., Shaw, S.L., 2013. Characterizing the isotopic composition of atmospheric ammonia emission sources using passive samplers and a combined oxidation-bacterial denitrifier approach. Rapid Communications in Mass Spectrometry 27 (20), 2239–2246.
Galloway, J.N., Townsend, A.R., Erisman, J.W., Bekunda, M., Cai, Z., Freney, J.R., Martinelli, L.A., Seitzinger, S.P., Sutton, M.A., 2008. Transformation of the nitrogen cycle: recent trends, questions, and potential solutions. Science 320 (5878), 889–892.
Granger, J., Sigman, D.M., Lehmann, M.F., Tortell, P.D., 2008. Nitrogen and oxygen isotope fractionation during dissimilatory nitrate reduction by denitrifying bacteria. Limnology & Oceanography 53 (6), 2533–2545.
Granger, J., Sigman, D.M., Rohde, M.M., Maldonado, M.T., Tortell, P.D., 2010. N and O isotope effects during nitrate assimilation by unicellular prokaryotic and eukaryotic plankton cultures. Geochimica et Cosmochimica Acta 74 (3), 1030–1040.
Granger, J., Wankel, S.D., 2016. Isotopic overprinting of nitrification on denitrification as a ubiquitous and unifying feature of environmental nitrogen cycling. Proceedings of the National Academy of Sciences 113 (42), E6391–E6400.
Groffman, P.M., Altabet, M.A., Böhlke, J.K., Butterbach-Bahl, K., David, M.B., Firestone, M.K., Giblin, A.E., Kana, T.M., Nielsen, L.P., Voytek, M.A., 2006. Methods for measuring denitrification: diverse approaches to a difficult problem. Ecological Applications 16 (6), 2091–2122.
Groffman, P.M., Holland, E.A., Myrold, D.D., Robertson, G.P., Zou, X., 1999. Denitrification. In: Robertson, G.P., Bledsoe, C.S., Coleman, D.C., Sollins, P. (Eds.), Standard Soil Methods for Long-term Ecological Research. Oxford University Press, New York, pp. 272–290.
Groffmann, P.M., Zak, D.R., Christensen, S., Mosier, A., Tiedje, J.M., 1993. Early spring nitrogen dynamics in a temperate forest landscape. Ecology 74 (5), 1579–1585.
Hall, S.J., Weintraub, S.R., Bowling, D.R., 2016. Scale-dependent linkages between nitrate isotopes and denitrification in surface soils: implications for isotope measurements and models. Oecologia 181 (4), 1221–1231.
Hart, S.C., Stark, J.M., Davidson, E.A., Firestone, M.K., 1994. Nitrogen mineralization, immobilization, and nitrification. In: Weaver, R.M., Bottomley, S., Bezdicek, P., Smith, D., Tabatabai, S., Wollum, A. (Eds.), Methods of Soil Analysis. Part 2: Microbiological and Biochemical Properties. Soil Science Society of America, Inc., Madison, WI, pp. 985–1018.
Högberg, P., Fan, H., Quist, M., Binkley, D.A.N., Tamm, C.O., 2006. Tree growth and soil acidification in response to 30 years of experimental nitrogen loading on boreal forest. Global Change Biology 12 (3), 489–499.
Houlton, B.Z., Sigman, D.M., Hedin, L.O., 2006. Isotopic evidence for large gaseous nitrogen losses from tropical rainforests. Proceedings of the National Academy of Sciences 103 (23), 8745–8750.
Inselsbacher, E., Wanek, W., Strauss, J., Zechmeister-Boltenstern, S., Müller, C., 2013. A novel ^{15}N tracer model reveals: plant nitrate uptake governs nitrogen transformation rates in agricultural soils. Soil Biology and Biochemistry 57, 301–310.
Kaiser, J., Hastings, M.G., Houlton, B.Z., Röckmann, T., Sigman, D.M., 2007. Triple oxygen isotope analysis of nitrate using the denitrifier method and thermal decomposition of N_2O. Analytical Chemistry 79 (2), 599–607.
Kaiser, J., Röckmann, T., Brenninkmeijer, C.A., 2004. Contribution of mass-dependent fractionation to the oxygen isotope anomaly of atmospheric nitrous oxide. Journal of Geophysical Research: Atmosphere 109 (D3).
Kang, H., Stanley, E.H., Park, S.S., 2003. A sensitive method for the measurement of ammonium in soil extract and water. Communications in Soil Science and Plant Analysis 34 (15–16), 2193–2201.
Keiluweit, M., Gee, K., Denney, A., Fendorf, S., 2018. Anoxic microsites in upland soils dominantly controlled by clay content. Soil Biology and Biochemistry 118, 42–50.
Kirkham, D.O.N., Bartholomew, W.V., 1954. Equations for following nutrient transformations in soil, utilizing tracer data 1. Soil Science Society of America Journal 18 (1), 33–34.
LeBauer, D.S., Treseder, K.K., 2008. Nitrogen limitation of net primary productivity in terrestrial ecosystems is globally distributed. Ecology 89 (2), 371–379.
Li, Y., Schichtel, B.A., Walker, J.T., Schwede, D.B., Chen, X., Lehmann, C.M., Puchalski, M.A., Gay, D.A., Collett, J.L., 2016. Increasing importance of deposition of reduced nitrogen in the United States. Proceedings of the National Academy of Sciences 113, 5874–5879.
Luz, B., Barkan, E., 2005. The isotopic ratios $^{17}O/^{16}O$ and $^{18}O/^{16}O$ in molecular oxygen and their significance in biogeochemistry. Geochimica et Cosmochimica Acta 69 (5), 1099–1110.
MacDonald, J.A., Dise, N.B., Matzner, E., Armbruster, M., Gundersen, P., Forsius, M., 2002. Nitrogen input together with ecosystem nitrogen enrichment predict nitrate leaching from European forests. Global Change Biology 8 (10), 1028–1033.
Maggi, F., Gu, C., Riley, W.J., Hornberger, G.M., Venterea, R.T., Xu, T., Spycher, N., Steefel, C., Miller, N.L., Oldenburg, C.M., 2008. A mechanistic treatment of the dominant soil nitrogen cycling processes: model development, testing, and application. Journal of Geophysical Research: Biogeosciences 113 (G2).
Mariotti, A., Germon, J.C., Hubert, P., Kaiser, P., Letolle, R., Tardieux, A., Tardieux, P., 1981. Experimental determination of nitrogen kinetic isotope fractionation: some principles; illustration for the denitrification and nitrification processes. Plant and Soil 62 (3), 413–430.
Mariotti, A., Landreau, A., Simon, B., 1988. ^{15}N isotope biogeochemistry and natural denitrification process in groundwater: application to the chalk aquifer of northern France. Geochimica et Cosmochimica Acta 52 (7), 1869–1878.
Mary, B., Recous, S., Robin, D., 1998. A model for calculating nitrogen fluxes in soil using ^{15}N tracing. Soil Biology and Biochemistry 30 (14), 1963–1979.
Mayer, B., Bollwerk, S.M., Mansfeldt, T., Hütter, B., Veizer, J., 2001. The oxygen isotope composition of nitrate generated by nitrification in acid forest floors. Geochimica et Cosmochimica Acta 65 (16), 2743–2756.
Michalski, G., Meixner, T., Fenn, M., Hernandez, L., Sirulnik, A., Allen, E., Thiemens, M., 2004. Tracing atmospheric nitrate deposition in a complex semiarid ecosystem using $\Delta^{17}O$. Environmental Science & Technology 38 (7), 2175–2181.
Michalski, G., Savarino, J., Böhlke, J.K., Thiemens, M., 2002. Determination of the total oxygen isotopic composition of nitrate and the calibration of a $\Delta^{17}O$ nitrate reference material. Analytical Chemistry 74 (19), 4989–4993.
Michalski, G., Scott, Z., Kabiling, M., Thiemens, M.H., 2003. First measurements and modeling of $\Delta^{17}O$ in atmospheric nitrate. Geophysical Research Letters 30 (16).
Miller, M.F., 2002. Isotopic fractionation and the quantification of ^{17}O anomalies in the oxygen three-isotope system: an appraisal and geochemical significance. Geochimica et Cosmochimica Acta 66 (11), 1881–1889.
Morin, S., Savarino, J., Frey, M.M., Domine, F., Jacobi, H.W., Kaleschke, L., Martins, J.M.F., 2009. Comprehensive isotopic composition of atmospheric nitrate in the Atlantic Ocean boundary layer from 65°S to 79°N. Journal of Geophysical Research 114 D05303.
Morse, J.L., Durán, J., Groffman, P.M., 2015. Soil denitrification fluxes in a northern hardwood forest: the importance of snowmelt and implications for ecosystem N budgets. Ecosystems 18 (3), 520–532.
Müller, C., Stevens, R.J., Laughlin, R.J., 2004. A ^{15}N tracing model to analyse N transformations in old grassland soil. Soil Biology and Biochemistry 36 (4), 619–632.
Myrold, D.D., Tiedje, J.M., 1986. Simultaneous estimation of several nitrogen cycle rates using ^{15}N: theory and application. Soil Biology and Biochemistry 18 (6), 559–568.
Oelmann, Y., Kreutziger, Y., Bol, R., Wilcke, W., 2007. Nitrate leaching in soil: tracing the NO_3^- sources with the help of stable N and O isotopes. Soil Biology and Biochemistry 39 (12), 3024–3033.
Osaka, K.I., Ohte, N., Koba, K., Yoshimizu, C., Katsuyama, M., Tani, M., Tayasu, I., Nagata, T., 2010. Hydrological influences on spatiotemporal variations of $\delta^{15}N$ and $\delta^{18}O$ of nitrate in a forested headwater catchment in central Japan: denitrification plays a critical role in groundwater. Journal of Geophysical Research: Biogeosciences 115 (G2).
Rice, C.W., Tiedje, J.M., 1989. Regulation of nitrate assimilation by ammonium in soils and in isolated soil microorganisms. Soil Biology and Biochemistry 21 (4), 597–602.
Riha, K.M., Michalski, G., Gallo, E.L., Lohse, K.A., Brooks, P.D., Meixner, T., 2014. High atmospheric nitrate inputs and nitrogen turnover in semi-arid urban catchments. Ecosystems 17 (8), 1309–1325.
Rose, L.A., Elliott, E.M., Adams, M.B., 2015. Triple nitrate isotopes indicate differing nitrate source contributions to streams across a nitrogen saturation gradient. Ecosystems 18 (7), 1209–1223.
Schenker, N., Gentleman, J.F., 2001. On judging the significance of differences by examining the overlap between confidence intervals. The American Statistician 55 (3), 182–186.
Schimel, J.P., Bennett, J., 2004. Nitrogen mineralization: challenges of a changing paradigm. Ecology 85 (3), 591–602.
Schimel, J.P., Jackson, L.E., Firestone, M.K., 1989. Spatial and temporal effects on plant-microbial competition for inorganic nitrogen in a California annual grassland. Soil Biology and Biochemistry 21 (8), 1059–1066.
Shi, W., Norton, J.M., 2000. Microbial control of nitrate concentrations in an agricultural soil treated with dairy waste compost or ammonium fertilizer. Soil Biology and Biochemistry 32 (10), 1453–1457.
Sigman, D.M., Casciotti, K.L., Andreani, M., Barford, C., Galanter, M.B.J.K., Böhlke, J.K., 2001. A bacterial method for the nitrogen isotopic analysis of nitrate in seawater and freshwater. Analytical Chemistry 73 (17), 4145–4153.
Singh, B.K., Bardgett, R.D., Smith, P., Reay, D.S., 2010. Microorganisms and climate change: terrestrial feedbacks and mitigation options. Nature Reviews Microbiology 8 (11), 779–790.
Smith, C.J., Chalk, P.M., Crawford, D.M., Wood, J.T., 1994. Estimating gross nitrogen mineralization and immobilization rates in anaerobic and aerobic soil suspensions. Soil Science Society of America Journal 58 (6), 1652–1660.
Snider, D., Thompson, K., Wagner-Riddle, C., Spoelstra, J., Dunfield, K., 2015. Molecular techniques and stable isotope ratios at natural abundance give complementary inferences about N_2O production pathways in an agricultural soil following a rainfall event. Soil Biology and Biochemistry 88, 197–213.
Stark, J.M., Hart, S.C., 1997. High rates of nitrification and nitrate turnover in undisturbed coniferous forests. Nature 385 (6611), 61–64.
Taylor, B.W., Keep, C.F., Hall Jr., R.O., Koch, B.J., Tronstad, L.M., Flecker, A.S., Ulseth, A.J., 2007. Improving the fluorometric ammonium method: matrix effects, background fluorescence, and standard additions. Journal of the North American Benthological Society 26 (2), 167–177.
Thiemens, M.H., 2006. History and applications of mass-independent isotope effects. Annual Review of Earth and Planetary Sciences 34, 217–262.
Tilman, D., Wedin, D., Knops, J., 1996. Productivity and sustainability influenced by biodiversity in grassland ecosystems. Nature 379 (6567), 718–720.
Young, E.D., Galy, A., Nagahara, H., 2002. Kinetic and equilibrium mass-dependent isotope fractionation laws in nature and their geochemical and cosmochemical significance. Geochimica et Cosmochimica Acta 66 (6), 1095–1104.
Yu, L., Zhu, J., Mulder, J., Dörsch, P., 2016. Multiyear dual nitrate isotope signatures suggest that N-saturated subtropical forested catchments can act as robust N sinks. Global Change Biology 22 (11), 3662–3674.
Yun, S.I., Ro, H.M., 2014. Can nitrogen isotope fractionation reveal ammonia oxidation responses to varying soil moisture? Soil Biology and Biochemistry 76, 136–139.
Zhang, L., Altabet, M.A., Wu, T., Hadas, O., 2007. Sensitive measurement of NH_4^+ $^{15}N/^{14}N$ ($\delta^{15}NH_4^+$) at natural abundance levels in fresh and saltwaters. Analytical Chemistry 79 (14), 5297–5303.
Zhang, S., Fang, Y., Xi, D., 2015. Adaptation of micro-diffusion method for the analysis of 15N natural abundance of ammonium in samples with small volume. Rapid Communications in Mass Spectrometry 29 (14), 1297–1306.